

(NASA-CR-188991) NUMERICAL PREDICTION OF
TURBULENT FLAME STABILITY IN
PREMIXED/PREVAPORIZED (HSCT) COMBUSTORS
Final Report, 1 Apr. 1989 - 31 Dec. 1990
(Maine Univ.) 75 p

N92-11161

Unclas
0048380

CSCL 21B G3/25

**NUMERICAL PREDICTION OF
TURBULENT FLAME STABILITY
IN PREMIXED/PREVAPORIZED
(HSCT) COMBUSTORS**

Nicholas S. Winowich
University of Maine
Orono, Maine

Final Report for
NASA Lewis Research Center
Grant No. NAG 3-1033
Period 4/1/89 - 12/31/90

ABSTRACT

A numerical analysis of combustion instabilities that induce flashback in a lean, premixed, prevaporized dump combustor is performed. KIVA-II, a finite volume CFD code for the modeling of transient, multidimensional, chemically reactive flows, serves as the principal analytical tool. The experiment of Proctor and T'ien [13] is used as a reference for developing the computational model. An experimentally derived combustion instability mechanism is presented on the basis of the observations of Proctor and T'ien and other investigators of instabilities in low-speed ($M < 0.1$) dump combustors. The analysis comprises two independent procedures that begin from a calculated stable flame: the first is a linear increase of the equivalence ratio and the second is the linear decrease of the inflow velocity. The objective is to observe changes in the aerothermochemical features of the flow field prior to flashback. It is found that only the linear increase of the equivalence ratio elicits a calculated flashback result. Though this result does not exhibit large-scale coherent vortices in the turbulent shear layer coincident with a flame flickering mode as observed experimentally, there are interesting acoustic effects which are resolved quite well in the calculation. A discussion of the $k - \epsilon$ turbulence model used by KIVA-II is prompted by the absence of combustion instabilities in the model as the inflow velocity is linearly decreased. Finally, recommendations are made for further numerical analysis that may improve correlation with experimentally observed combustion instabilities.

Table of Contents

ABSTRACT.....	i
TABLE OF CONTENTS.....	ii
LIST OF FIGURES.....	iv
OVERVIEW.....	1
CHAPTER 1-INTRODUCTION.....	3
1.1 Statement of Purpose.....	3
1.2 Literature Review.....	4
1.3 Combustion Instability Mechanism Revealed by Experiment.....	8
CHAPTER 2-ANALYTICAL METHODS.....	10
2.1 Experimental Basis.....	10
2.2 Computational Methods.....	10
2.3 Governing Equations.....	12
2.4 Preliminary Test of Computation Model.....	17
CHAPTER 3-MODEL DEFINITION.....	18
3.1 Computational Mesh.....	18
3.2 Boundary Conditions.....	18
3.3 Initial Conditions.....	20
CHAPTER 4-COMPUTATIONAL PROCEDURE.....	21
4.1 Start-Up.....	21
4.2 Calibration of the Chemical Kinetics Model.....	23
4.3 Simulations.....	24
CHAPTER 5-DISCUSSION OF RESULTS.....	26
5.1 Increased Equivalence Ratio.....	26
5.2 Decreased Inflow Velocity.....	29

CHAPTER 6-CONCLUSIONS AND RECOMMENDATIONS	32
6.1 Conclusions	32
6.2 Recommendations for Further Analysis	33
APPENDICES	57
REFERENCES	69

List of Figures

Figure No. & Caption	Page
1a. Experimental Apparatus, after Logan, et.al.	37
1b. Map of Dump Combustor Modes, after Logan, et.al.	37
2a. KIVA-II: Turbulent Flow Over a Step	38
2b. FIDAP: Turbulent Flow Over a Step	39
3a. Keller, et.al. Experiment- Stable Flame at Equivalence Ratio 0.57	41
3b. Numerical Model of Keller, et.al. Experiment	42
4a. Proctor and T'ien Experimental Apparatus	43
4b. Computational Mesh	43
5a. Proctor and T'ien Experimental Flashback Sequence	44
5b. Typical Combustor Pressure History, after Proctor and T'ien	45
6. Cold Flow Steady State Calculation	46
7. Stable Flame at Equivalence Ratio 0.44	47
8. Combustor Pressure History of Reactive Flow State-Up	48
9. Calculated Flashback Sequence	49
10. Combustor Pressure History of Flashback Sequence	55
11. Combustor Pressure History of Inflow Velocity is Decreased	56

OVERVIEW

A dump combustor is characterized by 1) the sudden expansion of a premixed, prevaporized fuel/air mixture over a rearward facing step or dump plane, and 2) combustion of this mixture across a flame front that is seated on the edge of the step. Combustion instabilities which disturb the flame have been investigated in many experiments using low-speed ($M < 0.1$) axisymmetric or rectangular dump combustors. One such experiment, conducted at the NASA Lewis Research Center by Proctor and T'ien [13], is used as a basis in this computational analysis of combustion instabilities leading to flashback, a condition in which the flame migrates upstream into the premixing region. In addition to expounding on this statement of purpose, Chapter 1 examines a few experiments which both predate and postdate that by Proctor and T'ien. A combustion instability mechanism evolving from these and other experimental investigations is outlined at the end of the chapter. It is important to understand each step in this mechanism since it is referred to repeatedly.

Chapter 2 is devoted to describing the analytical methods that are employed in this study. It begins by presenting results of the Proctor and T'ien experiment that are used in developing the numerical model. This is followed by a description of the ICED-ALE finite volume method implemented in the KIVA-II computer program. A summary of the governing equations of motion, turbulence, and chemical reaction solved by KIVA-II is also presented. Before setting up a computational model of the Proctor and T'ien experiment, two preliminary tests of the KIVA-II code are performed. A brief assessment of the results of these tests is made at the end of the chapter with reference to Figures 2 and 3.

Chapter 3 describes how the computational model is set up, beginning with the generation of the mesh based on the geometry of the Proctor and T'ien experimental rig. Details of the boundary conditions invoked at the inflow and outflow planes are presented. Also described is the law-of-the-wall boundary layer prescription that is used to model the velocity profile

and heat flux at the solid boundaries. Chapter 3 closes with an identification of the initial constituents and thermodynamic state of the fluid in the mesh.

Chapter 4 begins with a description of the cold flow calculation. Then the difficulties that arise during the calculation of ignition are discussed with comparisons made to the ignition procedure implemented by Proctor and T'ien. Following this is a description of the method used to calibrate the chemical kinetics model in KIVA-II so that flashback is calculated at approximately the same equivalence ratio as observed by Proctor and T'ien. Finally, the two-part procedure used to investigate combustion instabilities prior to flashback is described.

The results of this two-part procedure are presented and discussed in Chapter 5. The first part, which entails the linear increase of the equivalence ratio¹ from a calculated stable flame, does yield a flashback result. However, the second part of the procedure, which is the linear decrease of the inflow velocity from the same stable flame calculation, does not induce combustion instability or flashback in the numerical model. Suggested reasons for the disparity in these results are discussed.

Chapter 6 presents a summary of the experimentally observed reactive flow phenomena that the KIVA-II model simulates well. Also presented are the disparities between the calculated combustion instabilities and the experimentally observed mechanism outlined at the end of Chapter 1. Finally, recommendations are made for improving the acoustic and chemical modeling capabilities of the KIVA-II program. These recommendations would increase data storage and computing time, but should result in improved agreement with experimental observations.

1. In this analysis, the equivalence ratio is defined on a mass basis as the ratio of the actual to stoichiometric fuel/dry-air ratios.

CHAPTER 1

INTRODUCTION

1.1 Statement of Purpose

Oxides of nitrogen (NO_x) are known to be detrimental to the ozone layer. Stringent emission standards for these compounds have resulted in the investigation of new gas turbine combustor designs by NASA and private aeronautics companies. One such design is a lean, premixed, prevaporized (LPP) dump combustor. The development of this particular gas turbine combustor has been hindered by the occurrence of combustion instabilities which can cause the flame front to migrate into the premixing region, a phenomenon called flashback. Three redeeming features of the LPP dump combustor are simplicity of design, high combustion efficiency, and reduced NO_x emissions.

In addition to its aeronautical application, O.I. Smith, et.al. [1] illustrate by experiment the potential of the LPP dump combustor for waste incineration. Long residence times of high temperature combustion products in the recirculation zone formed behind the dump plane offer a means for 'high destruction and removal efficiencies' of hazardous waste. Understanding the instability mechanisms leading to flashback is of particular importance in this application since stable, coherent recirculation zones are required to ensure complete incineration.

Culick [2] notes that the term 'combustion instability' commonly used in the literature is misleading. He reasons that combustion processes themselves, though sometimes oscillatory, are in most instances stable. But when they are coupled with convective oscillations that are acoustic, hydrodynamic, or thermodynamic in origin, sustained pressure fluctuations can occur in the flow field, resulting in noise, vibration, and flame oscillation which are characterized as combustion instabilities.

Three mechanisms are repeatedly discussed in the literature as drivers of combustion instability in an LPP dump combustor:

- (1) *acoustic disturbances* that result from the fact that variable speed flow of an inviscid gas through a dump combustor may excite acoustic modes, each with their own frequency;
- (2) *hydrodynamic instabilities* ascribed to the growth, coupling, and convection of large-scale, coherent vortices in the shear layer downstream of the step;
- (3) *unsteady heat release oscillations* resulting from combustion wave propagation within the cores of large-scale vortices.

The objective of this study is to investigate the exact nature of the flow field pressure oscillations and other aerothermochemical conditions existing prior to and during flashback for low speed flows ($M < 0.1$) in a simple LPP dump combustor using KIVA-II, a recently developed computational fluid dynamics code [3]. An improved understanding of these flow field features may lead to clearer insight into which of the three instability mechanisms, or combination thereof, are principal drivers under given operating conditions.

1.2 Literature Review

Many experimental studies of combustion instabilities in an LPP dump combustor have been published. Some focus on the high speed ($M > 1$) instabilities that impede ramjet performance. However, for this analysis only those experiments that investigate instability in the combustion of low speed flows ($M < 0.1$ and $10^3 < Re < 10^4$) in an LPP dump combustor are considered.

Improved understanding of combustion instability has been derived largely from recent insight on the vortical dynamics of nonreacting turbulent shear layers. In the mid-1970's,

several investigators identified large-scale¹, coherent vortices as principal mechanisms in the development and growth of turbulent shear layers [4-6]. Later, Ganji and Sawyer [7] were among the first to study the development of large-scale vortices in both non-reacting and reacting turbulent flows in a dump combustor. By varying the diameter and location of a trip wire in the laminar boundary layer of the premixing region, they observe that the formation and growth rate of coherent vortices in the shear layer downstream is impaired when transition to turbulence occurs in the premixer boundary layer. In addition, they note that there is little difference in the incipient development and growth rate of vortices in reacting and non-reacting shear layers. Finally, they observe that flame structure and propagation is influenced by developing vortices since they entrain reactants at the top of the shear layer and induce combustion through subsequent mixing with hot products.

Keller, et.al. [8] investigate large-scale vortex movements and growth rates as instability mechanisms leading to flashback. They distinguish three levels of instability as the fuel mass flow rate is increased to the lean flashback limit. Each is associated with a pressure profile of distinct amplitude and frequency which is evidenced by noise characterized as humming, buzzing, and chucking. Accompanying each sound change is an increased level of flame oscillation laterally across the combustion zone. The humming is ascribed to longitudinal standing waves associated with the natural frequencies of the dump combustor, an acoustic effect. The buzzing and chucking are more energetic and are said to be produced by the growth and convection of large-scale vortices in the shear layer, a hydrodynamic effect. When chucking occurs, the convective oscillations produced by the action of large-scale vortices in the initial region of the shear layer induce flow reversals in the boundary layer just upstream of the step. This enables the flame front to detach from the corner of the step and migrate upstream through the premixer boundary layer, giving rise to flashback.

1. 'Large-scale' connotes vortical diameters that are many times larger than the length scale of turbulent eddies. These vortices span an identifiable, and often major, portion of the width of the turbulent shear layer.

The experimental results of Smith and Zukoski [9] reveal that large-scale vortices form only at resonant frequencies of the combustor and that combustion within these vortices as they grow and convect downstream induces a periodic heat release rate. They note that, in accordance with the Rayleigh criterion [10], when a constructive phase relationship exists between flow field pressure oscillations and the heat release rate, the acoustic field is excited. If enough energy is added to the acoustic field, large velocity fluctuations result which drive the flame off the corner of the step. This is most likely analogous to the 'chucking' effect in the Keller, et.al. experiment.

Schadow, et.al. [11] describe a driving mechanism for combustion instability that is similar to that of Smith and Zukoski. In addition, they propose that combustion occurs first at the circumference of any given large-scale vortex and propagates inward, resulting in the periodic heat release. Schadow, et.al. also note that a turbulent shear layer has associated with it a range of hydrodynamic instability frequencies. In its initial region, the shear layer develops instability waves whose frequencies are a function of the flow structure in the boundary layer upstream of the step as described in references [4-6] and [7]. Further along in the shear layer are instabilities that are subharmonics of the initial shear layer instability frequency. The size that vortices achieve as they convect downstream is determined by the frequency at which the most constructive phase relationship occurs between the shear layer instabilities and the system resonance mode. Schadow, et.al. conclude that decoupling these oscillatory mechanisms, particularly when the development of large-scale vortices is favored, could be a means of damping the large pressure oscillations that drive combustion instability. (It is important to note that, in contrast to the other experiments described herein, Schadow, et.al. investigate a *diffusion* flame in a dump combustor. However, in considering the qualitative effects of large-scale vortices on combustion instability, it is assumed that there is little or no distinction between premixed and diffusion flames.)

Logan, et.al. [12] have developed a very interesting experimental dump combustor in which they are able to adjust the length (l_c) to height (h_c) aspect ratio of the combustion chamber using movable ceramic plugs at the exit (Figure 1a). They distinguish three modes of instability at various combinations of combustion chamber geometry and equivalence ratio (Figure 1b). The first is a low-frequency (30-50Hz) 'chugging' mode in which a single vortex pair periodically develops at the dump plane and grows to fill the entire combustor cavity, precluding the establishment of a stable recirculation zone. The other two modes, distinguished as 'A' and 'B', are at much higher frequencies (mode A:600-700Hz, mode B:350-600Hz) and elicit the simultaneous occurrence of a few or several vortex pairs in the combustion chamber. A coherent recirculation zone is maintained at these high frequency modes. Between the shaded regions in Figure 1b are quiescent conditions in which the recirculation zone is unperturbed. One of the most revealing insights of this experimental study is the effect of the acoustic field on the appearance of combustion instabilities and on the potential for modulating them with adjustments to the combustion chamber geometry.

An experimental investigation of flame flashback in an LPP dump combustor is also done by Proctor and T'ien [13] at NASA's Lewis Research Center. They propose a flashback mechanism similar to that of Keller, et.al. which entails the propagation of the flame upstream through the premixer boundary layer. At first, this appears to be a reaffirmation of the 'classical' flashback mechanism of Lewis and von Elbe which relates the flame speed to the mean velocity in the boundary layer of a Bunsen burner tube [21]. However, Proctor and T'ien observe that lower equivalence ratios are required for incipient flashback as the premixer velocity is increased. Since flame speed increases with equivalence ratio, Proctor and T'ien conclude that a different flashback mechanism exists in a dump combustor. Consistent with their observations, they propose that flow reversals in the premixer boundary layer elicited by high amplitude combustor pressure oscillations actuate upstream flame propagation. This experiment is discussed in more detail in the next chapter.

1.3 Combustion Instability Mechanism Revealed by Experiment

The increased amplitude of combustor pressure oscillations is consistently observed to be coincident with flame flickering and, in the most extreme case, flashback in a dump combustor. Some of the experiments described in the previous section have examined the vortical dynamics of reacting turbulent shear layers in conjunction with system resonance modes to explain the development of these high amplitude pressure oscillations. The following outline serves as a summarized combustion instability mechanism based on the experimental work cited in the previous section and in references [18-20]:

- (1) an acoustic field exists with fundamental and harmonic frequencies unique to the combustor geometry;
- (2) turbulent shear layer instability waves exist whose frequencies are a function of the velocity profile and flow structure of the boundary layer just upstream of the dump plane;
- (3) a constructive phase relationship arises at one or more frequencies common to the shear layer and acoustic field, leading to the development of coherent vortices;
- (4) combustion within the vortices as they grow and convect downstream results in a periodic heat release rate which intensifies the acoustic field;
- (5) the stronger acoustic field favors development of larger vortices which, in turn, amplify the heat release oscillations;
- (6) self-excited oscillations in the 'closed loop' mechanism of steps (1)-(5) cause high amplitude pressure oscillations that ultimately drive the flame upstream into the premixer with its leading edge in the premixer boundary layer.

An understanding of the parameters controlling the occurrence of step (3) is essential since

large-scale vortices elicit oscillations in the heat release rate. Experiment has cited fuel type, equivalence ratio, premixer Reynolds number, and combustor geometry as controlling parameters in the development of coherent vortices in the shear layer. In this analysis, combustor geometry and fuel type are fixed while the equivalence ratio and the premixer Reynolds number are varied independently from a stable flame solution. It is important that each step in the experimentally observed instability mechanism outlined above be understood since it is frequently referenced in this analysis.

CHAPTER 2

ANALYTICAL METHODS

2.1 Experimental Basis

The experimental work by Proctor and T'ien serves as a basis for this computational analysis. In this experiment, inlet air temperature, premixer wall temperature, and average premixer velocity are varied parametrically to determine their individual effects on the minimum equivalence ratio required for sustained flashback. The results of their parametric study are:

- (1) the effect of inlet air temperature is 'slight';
- (2) premixer wall temperature is said not to be an important parameter in the occurrence of flashback;
- (3) as the average premixer velocity is increased, lower equivalence ratios are required for flashback.

Proctor and T'ien conclude that flashback is induced by flow reversals in the boundary layer at the premixer exit. These flow reversals are most likely generated by pressure oscillations in the combustion chamber which are observed to reach a maximum amplitude just before flashback. Flame flickering prior to flashback, perhaps caused by large-scale vortices shedding from the step, is considered a visible sign of the increased amplitude of the oscillations (Figure 5a+b).

2.2 Computational Methods

The KIVA-II computer program developed at Los Alamos National Laboratory is used. It solves the governing equations for transient, multidimensional, chemically reactive flow using a combined Implicit Continuous-flow Eulerian and Arbitrary Lagrangian-Eulerian

(ICEd-ALE) finite volume method. The synergistic pairing of the ICE and ALE methods enable KIVA-II to model a wide range of flows at all speeds (ICE) in arbitrary geometries (ALE). By itself, the ALE method has two advantages: 1) a deformable mesh comprised of hexahedrons whose vertices are arbitrarily specified functions of time, and 2) quick convergence of the explicit solution procedures for high speed flows. A disadvantage, however, is that for low speed flows the Courant sound speed stability criterion is extremely restrictive on the time step. By combining the implicit calculation of pressure in the ICE method with the ALE method, the stringency of the Courant condition is removed so that low speed flows can be calculated efficiently.

The ICEd-ALE method comprises three phases. Phase A is an explicit calculation that solves the Lagrangian conservation equations for mass and momentum as a couple. The Lagrangian volumes that result are used to solve the energy equation, yielding the time $n+1$ internal energies. Finally in Phase A, the time $n+1$ pressures are computed from the equation of state. For high speed flows in which a completely explicit calculation is acceptable, Phase A would, by itself, give a solution. For low speed flows, however, the implicit calculation of Phase B is necessary so that pressure signals may traverse more than one cell in a time step. Using the Lagrangian velocities determined in Phase A as a first guess, Phase B invokes mass conservation as it implicitly updates the pressure, density, and Lagrangian velocities according to the ICE method. Then, just as in Phase A, time $n+1$ internal energy and pressure are obtained from the solution of the energy and state equations.

Since Phases A and B actuate a purely Lagrangian description of the flow field, mesh vertices move at the local fluid velocity, preventing advection across cell boundaries. In Phase C, called the rezone phase, explicit solution methods are used to fix the flow field, move the vertices to new locations, and then remap or 'rezone' the flow field onto the new mesh by advecting mass, momentum, and energy across cell boundaries. In this way Phase

C effectively undoes some or all of the changes to the shape of the mesh that occur in the Lagrangian calculations of Phases A and B. Since a continuous flow device with immovable boundaries is considered in this analysis, Phase C maintains a fixed computational mesh by moving vertices back to their original positions every time step for a purely Eulerian description of the flow field.

In the ICED-ALE method, equations are differenced in integral form using the volume of a typical computational cell as a control volume. Divergence terms are transformed to surface integrals using the divergence theorem [3].

2.3 Governing Equations

An overview of the governing equations solved by the ICED-ALE finite volume scheme follows. Note that $\vec{\nabla}$ is the three dimensional del operator defined as:

$$\vec{\nabla} = i \frac{\partial}{\partial x} + j \frac{\partial}{\partial y} + k \frac{\partial}{\partial z} .$$

Conservation Equations

Continuity:

$$\frac{\partial \rho_m}{\partial t} + \vec{\nabla} \cdot (\rho_m \vec{u}) = \vec{\nabla} \cdot \vec{J}_m + \dot{\rho}_m^c$$

for the m th species, where ρ_m is the mass density of species m , \vec{u} is the fluid velocity, \vec{J}_m is the diffusive mass flux of species m , and $\dot{\rho}_m^c$ is the rate of change of ρ_m due to chemical reaction. The diffusive mass flux is given by Fick's Law:

$$\vec{J}_m = \rho D \vec{\nabla} Y_m$$

where ρ is the total mass density and Y_m is the species mass fraction. The mass diffusivity

D is assumed to be the same for all species since turbulence is the dominant mechanism for mass diffusion. It is computed using the Schmidt number Sc and viscosity μ :

$$D = \frac{\mu}{\rho Sc} .$$

By summing over all species, the total mass density equation is:

$$\frac{\partial \rho}{\partial t} + \vec{\nabla} \cdot (\rho \vec{u}) = 0$$

since mass is conserved in diffusion and chemical reaction.

Momentum:

$$\frac{\partial (\rho \vec{u})}{\partial t} + \vec{\nabla} \cdot (\rho \vec{u} \vec{u}) = -\vec{\nabla} p - \vec{\nabla} \rho k + \vec{\nabla} \cdot \sigma$$

where p is the fluid pressure, and k is the specific turbulent kinetic energy. The viscous stress tensor is Newtonian and is expressed as:

$$\sigma = \mu [\vec{\nabla} \vec{u} + (\vec{\nabla} \vec{u})^T] + \lambda \vec{\nabla} \cdot \vec{u} \underline{U}$$

where μ and λ are the shear and bulk viscosity coefficients, \underline{U} is the unit dyadic tensor, and superscript T denotes the transpose. The viscosity coefficients are given by:

$$\mu = \mu_{air} + c_{\mu} \rho \frac{k^2}{\epsilon}$$

and

$$\lambda = -\frac{2}{3} \mu$$

where ϵ is the specific turbulent kinetic energy dissipation rate and c_{μ} is an empirical turbulence constant equalling 0.09. A Sutherland formula is used for the molecular viscosity of air with A_1 and A_2 constant:

$$\mu_{air} = \frac{A_1 T^{3/2}}{T + A_2} .$$

Internal Energy Transport

The transport of internal energy ρI is governed by:

$$\frac{\partial(\rho I)}{\partial t} + \vec{\nabla} \cdot (\rho \vec{u} I) = -p \vec{\nabla} \cdot \vec{u} - \vec{\nabla} \cdot \vec{q} + \rho \varepsilon + Q^c$$

where Q^c is a source term due to chemical heat release. The heat flux \vec{q} , is gained by summing the effects of heat conduction and enthalpy transport by mass diffusion:

$$\vec{q} = \vec{q}_c + \vec{q}_d = -K \vec{\nabla} T - \sum_m h_m \vec{j}_m$$

where K is the thermal conductivity, T is the fluid temperature, and h_m is the species specific enthalpy. The thermal conductivity is determined using the Prandtl number Pr :

$$K = \frac{\mu c_p}{Pr}$$

where c_p is the specific heat at constant pressure. Finally, $\rho \varepsilon$ is the rate of internal energy production from turbulent kinetic energy dissipation.

Turbulence Equations

A two-equation k - ε turbulence model is used. It solves the following pair of equations for the turbulent kinetic energy ρk , and the turbulent kinetic energy dissipation rate $\rho \varepsilon$, respectively:

$$\frac{\partial \rho k}{\partial t} + \vec{\nabla} \cdot (\rho \vec{u} k) = -\frac{2}{3} \rho k \vec{\nabla} \cdot \vec{u} + \sigma : \vec{\nabla} \vec{u} + \vec{\nabla} \cdot \left[\frac{\mu}{Pr_k} \vec{\nabla} k \right] - \rho \varepsilon$$

$$\frac{\partial \rho \varepsilon}{\partial t} + \vec{\nabla} \cdot (\rho \vec{u} \varepsilon) = \left[-\left(\frac{2}{3} c_{\varepsilon_1} - c_{\varepsilon_3}\right) \rho \varepsilon \vec{\nabla} \cdot \vec{u} + \vec{\nabla} \cdot \left[\frac{\mu}{Pr_\varepsilon} \vec{\nabla} \varepsilon \right] + \frac{\varepsilon}{k} \left[c_{\varepsilon_1} \sigma : \vec{\nabla} \vec{u} - c_{\varepsilon_2} \rho \varepsilon \right] \right]$$

where c_{ε_1} , c_{ε_2} , c_{ε_3} , Pr_k , and Pr_ε are empirical constants having the following values [14]:

$$\begin{aligned}
 c_{\epsilon_1} &= 1.44 & Pr_k &= 1.0 \\
 c_{\epsilon_2} &= 1.92 & Pr_\epsilon &= 1.3 \\
 c_{\epsilon_3} &= -1.0 .
 \end{aligned}$$

With values for k and ϵ , the turbulent length scale L is computed directly from:

$$L = c_{\mu_\epsilon} \frac{k^{3/2}}{\epsilon}$$

where

$$c_{\mu_\epsilon} = \left[\frac{c_\mu}{Pr_\epsilon (c_{\epsilon_2} - c_{\epsilon_1})} \right]^{1/2} .$$

Chemical Equations

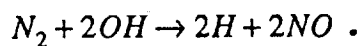
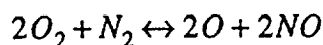
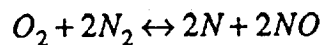
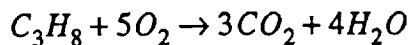
Gaseous mixtures are assumed to behave as ideal gases and therefore conform to the equation of state:

$$p = R_u T \left(\sum_m \frac{\rho_m}{W_m} \right)$$

where W_m is the molecular weight of species m and R_u is the universal gas constant.

Chemical kinetics model:

Using propane (C_3H_8) as fuel, four kinetic reactions are considered:



A global reaction rate mechanism is employed to approximate the effects of the many

elementary steps associated with each of these reactions. The global rate expression is:

$$\dot{\omega}_{global} = k_{fr} \prod_n \left(\frac{\rho_n}{W_n} \right)^{b'_{nr}} - k_{br} \prod_m \left(\frac{\rho_m}{W_m} \right)^{a'_{mr}}$$

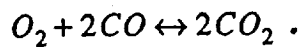
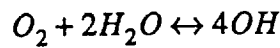
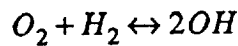
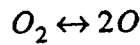
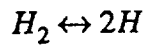
where a'_{mr} and b'_{nr} may be the stoichiometric coefficients of reactants m and products n in the four kinetic reactions considered or may be empirical constants determined from experiment or detailed kinetics calculations [15]. The forward and backward reaction rate coefficients k_{fr} and k_{br} for reaction r are determined from the Arrhenius expression:

$$k = AT^\zeta \exp\left(\frac{-E_a}{R_u T}\right).$$

The temperature exponent ζ , the activation energy E_a , and the pre-exponential term A , are also determined from correlation with experimental results in reference [15].

Equilibrium chemistry model:

Six equilibrium reactions are considered:



The rates of each equilibrium reaction above are determined implicitly from:

$$\prod_m \left(\frac{\rho_m}{W_m} \right)^{v''_{mr} - v'_{mr}} = K_c^r(T)$$

where v'_{mr} and v''_{mr} are the stoichiometric coefficients of species m on the left and right

side, respectively, of each reaction and $K_c^r(T)$ is the known equilibrium constant.

2.4 Preliminary Test of Computational Model

KIVA-II was originally developed to model the confined flows of internal combustion engines. Subsequent code modifications have added an inflow/outflow capability for gas turbine applications. To substantiate these changes, preliminary analyses of two flow regimes are conducted. The first is a non-reacting turbulent flow over a step. Using identical Reynolds numbers, turbulence parameters, and computational meshes, the results of the KIVA-II program are qualitatively similar to those of the FIDAP code developed and marketed by Fluid Dynamics International, Inc. (Figure 2a+b). It should be noted that the disparity in the numerical values accompanying the KIVA-II and FIDAP graphical output for this calculation occurs because KIVA-II uses the CGS system of units while FIDAP uses nondimensionalized variables. A direct quantitative comparison is difficult since the nondimensionalization parameters used in the FIDAP simulation are not specified. However, it can be seen that the KIVA-II and FIDAP simulations yield the same order of magnitude for the difference between maximum and minimum values of corresponding flow field quantities.

The Keller, et.al. experiment, introduced in section 1.2, is used as a second test. Figure 3a shows cinematographic schlieren records of a stable flame at an equivalence ratio of 0.57. With corresponding mesh geometry, boundary and initial conditions, fluid properties, Reynolds number, and turbulence parameters, KIVA-II yields the solution shown in Figure 3b. This solution is at steady state with virtually no combustor pressure oscillations, which contrasts with the highly transient nature of the experimental flame. The $k - \epsilon$ turbulence model used in KIVA-II does not appear to simulate the chaotic undulation of the flame in the latter part of the combustor. This shortcoming is discussed further in Chapter 5 with regard to the combustion model of the Proctor and T'ien experiment.

CHAPTER 3

MODEL DEFINITION

3.1 Computational Mesh

Calculation is made in two dimensions on the centrally located x-z plane ($y=0.0\text{in.}$) of the Proctor and T'ien experimental dump combustor (Figure 4a). Flow in this plane is symmetric about $x=0.0\text{in.}$ and, for this analysis, calculation occurs only in the lower half (Figure 4b). To properly model the incompressible flow resistance, the cross-sectional area ratio of the combustor to exhaust aperture in the computational mesh (A^*/B^*) closely approximates the corresponding ratio for the experimental dump combustor (A/B):

$$\frac{A}{B} = 5.093 \qquad \frac{A^*}{B^*} = 5.333 .$$

Proper dimensioning of the premixer and combustor place a restriction on the transverse (x) cell dimension in the computational mesh. This restriction forces the cross-sectional area ratio of the mesh to be slightly higher than the corresponding experimental value. (Note: The KIVA-II computer program, in original form, does not accommodate a symmetry plane in Cartesian meshes. Appendix B shows the four places in the code where modifications are made so that a symmetry plane can be utilized in this analysis.)

3.2 Boundary Conditions

Solid Boundaries

At the walls of the dump combustor, normal components of velocity are set to zero. To determine the tangential velocity components, the turbulent boundary layer is considered in two parts, separated by a critical Reynolds number R_c . The first part is the laminar

sublayer adjacent to the wall whose non-dimensional velocity profile is defined as:

$$\frac{u}{u^*} = \zeta^{1/2} \quad (\zeta \leq R_c) .$$

ζ is the Reynolds number based on gas velocity u relative to the wall evaluated a distance y from the wall:

$$\zeta = \frac{\rho y u}{\mu_{air}(T)} .$$

u^* , called the wall-friction velocity, results from the dimensional analysis of $u = u(\mu, \tau_w, \rho, y)$ where τ_w is the wall shear stress. Its value is determined by:

$$u^* = \left[\frac{\tau_w}{\rho} \right]^{1/2} .$$

In the second part of the two-part boundary layer model, the turbulent overlap and outer layers are combined. Here, the law-of-the-wall formulation is used in conjunction with the one-seventh power law to define the non-dimensional velocity profile:

$$\frac{u}{u^*} = \frac{1}{\kappa} \ln(c_{lw} \zeta^{7/8}) + B \quad (\zeta > R_c)$$

where $c_{lw} = 0.15$, $B = 5.5$, and Karmann constant $\kappa = 0.4327$. The critical Reynolds number R_c , determined by equating the two expressions above for $\frac{u}{u^*}$, is 114.

Isothermal walls are chosen for the dump combustor model based on the experimental setup of Proctor and T'ien. The wall heat flux J_w , using the two part boundary layer treatment above, is:

$$\frac{J_w}{\rho u^* c_p (T - T_w)} = \begin{cases} 1 / (Pr_l \frac{u}{u^*}) & (\zeta \leq R_c) \\ 1 / \left[Pr \left[\frac{u}{u^*} + \left(\frac{Pr_l}{Pr} - 1 \right) R_c^{1/2} \right] \right] & (\zeta > R_c) \end{cases}$$

where Pr_l is the fluid Prandtl number in the laminar sublayer and T_w is the wall

temperature.

Symmetry Plane

At the symmetry plane, a free slip condition is imposed on tangential components of velocity while normal components are set to zero. The symmetry plane is adiabatic and impervious to the transport of mass, momentum, and turbulent kinetic energy.

Inflow - Outflow

Beyond the inflow and outflow boundaries, fluid transport is assumed isentropic. Species densities and mixture pressure and temperature at the inlet and outlet planes are related to corresponding stagnation quantities using the equation of state and the isentropic relation:

$$\frac{\rho_o}{\rho} = \left[\frac{p_o}{p} \right]^{1/\gamma}$$

where γ is the ratio of specific heats. Turbulence quantities at the inflow and outflow boundaries are also related to corresponding stagnation values.

3.3 Initial Conditions

Species densities and mixture pressure and temperature are prescribed using the equation of state in three separate regions: 1) upstream of the premixer inlet; 2) the dump combustor flow field; and 3) downstream of the combustor exit. Dry-air ($O_2 + 3.76N_2$) exists at rest in the combustor at the beginning of each program run.

CHAPTER 4

COMPUTATIONAL PROCEDURE

4.1 Start-up

Cold Flow

A steady state cold flow calculation is made first (Figure 6). This is achieved quickly since the geometry of the mesh is simple. An important note regarding this and further calculations is that the pressure gradient scaling (PGS) method provided with the KIVA-II code is not used. The purpose of this method is to improve the efficiency in the calculation of low speed flows by narrowing the difference between the acoustic and convective time scales so that the Courant sound speed stability condition is more easily satisfied. This is achieved by lowering the sound speed in the fluid by a factor α , called the PGS parameter. Though the PGS method improves the efficiency of low speed implicit calculations significantly, it sacrifices accuracy in the modeling of acoustic disturbances. Since such disturbances are an important aspect of the combustion instability mechanism described in section 1.3, the PGS method is not implemented.

The Reynolds number based on the hydraulic diameter of the premixer varies with the velocity, temperature, and equivalence ratio of the incoming mixture. Using the kinematic viscosity of air at the inlet temperature, the Reynolds number is on the order of 10^3 for all inputs of velocity and equivalence ratio in this study, which corresponds to a turbulent flow regime.

Fuel Injection and Ignition

The existence of the exit plate at the end of the mesh makes ignition difficult because it creates a semi-confined flow field that often induces large amplitude pressure fluctuations

during ignition which, in turn, inhibit the formation of a stable flame on the corner of the step. In the experiment this problem is avoided by turning on the igniter at the same time as the fuel is injected and then increasing the equivalence ratio to a stable flame regime in no less than 30 seconds [Proctor, personal correspondence]. This prevents a buildup of fuel in the combustion chamber prior to and during ignition. Unfortunately, performing a calculation to 30 seconds requires excessive computing time even on a Cray-XMP. To circumvent this difficulty, the pre-exponential factor in the Arrhenius expression for the fuel oxidation reaction is linearly increased in time. This control of the energy release from combustion is a means of avoiding rapid temperature increases that, in turn, cause extreme pressure changes.

Fuel injection is accomplished by changing the stagnation densities upstream of the inlet plane so that propane is added to the dry-air mixture at a specified equivalence ratio. A cold flow steady state velocity field comprising only dry-air is always achieved prior to fuel injection and ignition. (Note: The quick equilibrium solver CHMQGM in KIVA-II requires trace amounts of H_2O and CO_2 in every cell to avoid divide-by-zero errors. These compounds are included at partial densities on the order of 10^{-25} in the cold flow mixture to fulfill this requirement.)

Ignition is approximated in the computational model by adding specific internal energy to the fluid in a preselected group of cells for a specified time interval. The rate of heat addition is controlled by an input parameter. It is found that a four percent increase per time step (compounded every time step) produces a successful ignition for the equivalence ratios considered in this study ($0.4 \leq \Phi \leq 0.7$).

A fourth-order node coupler is provided with the KIVA-II code to smooth velocity fluctuations that may arise during the Lagrangian portion of the ICED-ALE solution procedure. Though the node coupler is not needed to achieve a good steady state cold flow

solution, it is used during the combustion phase of the calculation to smooth velocity fluctuations that appear near the exit.

4.2 Calibration of the Chemical Kinetics Model

Proctor and T'ien find that a stable flame attached to the dump plane at the end of the premixer occurs under the following conditions:

- (1) inlet air temperature - 850K
- (2) premixer wall temperature - 750K
- (3) average premixer velocity - 2133 cm/sec
- (4) equivalence ratio - 0.44
- (5) Reynolds number based on premixer channel width - 6562¹

As the equivalence ratio is raised from 0.44, they observe an increase in the amplitude of combustor pressure oscillations. A maximum amplitude is reached just prior to flashback at an equivalence ratio of 0.56 (Figure 5a+b).

In order to achieve flashback under the same conditions in this numerical analysis, it is necessary to calibrate the chemical kinetics model by varying the pre-exponential factor in the Arrhenius expression for the reaction rate coefficient of the fuel oxidation reaction. For the combustion of C_3H_8 , Westbrook and Dryer [15] specify a pre-exponential factor of 8.6×10^{11} , noting that this value yields flame speeds that correlate well with experimental data. They also note, however, that global reaction rate mechanisms can vary with the type of experiment or combustion environment. In this analysis, a stable flame cannot be achieved under the conditions cited above with a pre-exponential factor of 8.6×10^{11} .² Using smaller values with the same order of magnitude, a stable flame is established. Then, upon

1. Using kinematic viscosity of air at 800K, 101.3 kPa.

2. It is noted in Chapter 5 that when using the quasi-second order upwind differencing scheme provided with the KIVA-II code, a stable flame can be calculated with the pre-exponential factor equalling 8.6×10^{11} . However, for reasons also described in Chapter 5, the partial donor-cell differencing scheme is used in nearly all computations.

raising the equivalence ratio, it is found that the occurrence of flashback is strongly dependent on the pre-exponential factor. This is to be expected since the fuel oxidation reaction is the dominate source of heat in the kinetics model and that the pre-exponential factor strongly influences the rate of heat release. A value of 1.9×10^{11} is chosen as a benchmark pre-exponential factor since it yields a stable flame at an equivalence ratio of 0.44 (Figure 7) and also elicits flashback at approximately 0.57, in good agreement with the Proctor and T'ien experiment.¹

As mentioned in the previous section, the pre-exponential factor is linearly increased in time during ignition. Prior to this the pre-exponential factor was held fixed and this caused a severe pressure spike in the combustor that immediately drove the flame into the premixer. Figure 8 shows a more moderate pressure rise brought on by the rapid increase in the rate of combustion as the bulk fluid temperature rises. Note that the stable flame calculation exhibits acoustic oscillations which are most likely a result of the ignition. (That these oscillations are acoustic is shown in Appendix C).

Premature flashback is also induced if the equivalence ratio is raised too quickly from the stable flame calculation of Figure 7. In the interest of computational efficiency, the time rate of increase in equivalence ratio is chosen to be 0.1 per second, a value slightly lower than the minimum necessary to avoid influencing the flashback result. Any further decrease in the rate of equivalence ratio ramping does not affect the occurrence of flashback.²

4.3 Simulations

Beginning from the stable flame calculation of Figure 7, two independent computations are

-
1. At this point in the analysis, a run is made to determine if the stable flame calculation of Figure 7 is mesh dependent. The aspect ratio (length/width) of the cells is changed from 2:1 to 1:1 making the mesh more coarse, and there is no difference in the result over that appearing in Figure 7.
 2. A calculation is made using a value of 0.05 per second for the rate of increase in the equivalence ratio, but there is no change in the flashback result over that when using a value of 0.1 per second.

performed. First, the equivalence ratio is linearly increased and second, the inflow velocity is linearly decreased. Since the inlet air temperature and premixer wall temperature are found by experiment not to be important parameters in the development and sustenance of flashback, they are not varied in this study. The goal is to:

- (1) investigate pressure oscillations and other aerothermochemical conditions in the flow field prior to flashback; and,
- (2) investigate vorticity as the flame becomes unstable.

The flashback observed by Proctor and T'ien as a result of raising the equivalence ratio has been discussed in the previous section with reference to Figures 5a+b. Proctor and T'ien also induce flashback by decreasing the average premixer velocity from 2621 cm/sec to 2316 cm/sec when the inlet air temperature is 830K, the premixer wall temperature is 750K, and the equivalence ratio is held fixed at 0.48. In the interest of computational efficiency, the linear decrease of the inflow velocity in the numerical calculation begins from the stable flame result of Figure 7 rather than computing a new stable flame using the experimental conditions cited above. This approximation is deemed valid, particularly since the inlet air temperature and the premixer wall temperature are observed not to significantly influence the occurrence of flashback.

Calculated results occur in a variety of useful forms: a) contour plots of pressure, temperature, and equivalence ratio in the flow field at specified times, b) time history plots of pressure, temperature, and equivalence ratio at prescribed locations in the flow field, c) streamline plots of the flow field downstream of the step and, d) printed output of aerothermochemical data for all computational cells.

CHAPTER 5

DISCUSSION OF RESULTS

5.1 Increased Equivalence Ratio

Figure 9 shows a calculated flashback sequence which is generated by linearly increasing the equivalence ratio from the stable flame value of $\Phi = 0.44$. A characteristic feature of impending flashback is the partitioning of the hot, diffuse region downstream of the high temperature gradient 'cone' (Figure 9a). This is followed by a collapse of the 'cone' into the premixer (Figure 9b-i). Note that this sequence occurs very rapidly (approx. 0.04 seconds), as expected. Also shown in Figure 9 is a sequence of nine streamline plots representing the same elapsed times in the calculation as the nine temperature contour plots. A disappointing feature of the streamline plots is the absence of coherent vortices in the turbulent shear layer extending from the dump plane. The occurrence of these vortices is predicted in step (3) of the combustion instability mechanism described in section 1.3. Of course, without this step, unsteady heat release oscillations do not develop and the self-excited, 'closed loop' character of the mechanism can never be sustained.

Figure 10 shows the combustor pressure history during flashback which includes the sequence of Figure 9. The amplitude of the acoustic disturbances increases approximately 30%¹ as the equivalence ratio is raised from 0.44 and then becomes irregular just prior to flashback. As flashback occurs a pressure jump is seen in the combustor, as expected. The amplitude of the pressure oscillations in this calculated result is substantially lower than during the onset of flashback in the Proctor and T'ien experiment (Figure 5b). It is possible that the higher amplitude oscillations seen in the experiment are a manifestation of the growth and convection of large-scale coherent vortices in the shear layer. Combustion

1. This percentage is calculated by comparing the change in amplitude of the acoustic oscillations from the stable flame regime of Figure 8 to that of impending flashback observed in Figure 10.

within the vortices may then have caused unsteady heat release oscillations as described in step (4) of the instability mechanism in section 1.3. This could have been the driving mechanism for the flame flickering mode that Proctor and T'ien observe prior to flashback. Note that Proctor and T'ien do not propose this as a driving mechanism for the combustion instabilities they observe since their work predates that of Smith and Zukoski [9], Schadow, et.al. [11], Logan, et.al. [12], and others [18-20] which has been essential to the evolution of the instability mechanism of section 1.3.

As a possible explanation for the aforementioned disparity in the calculated and experimental pressure oscillations prior to flashback, it should be noted that Proctor and T'ien raise the equivalence ratio from 0.44 up to the flashback limit of 0.60 in an elapsed time of a few minutes [Proctor, personal correspondence] while the calculated result has Φ raised from 0.44 to 0.57 in approximately 1.1 seconds. This being so, there may not be the opportunity for coherent vortices to form in the shear layer of the computational model. As mentioned at the end of section 4.2 the rate of equivalence ratio ramping is lowered from 0.1 per second (the value used to calculate the flashback sequence of Figure 9) to 0.05 per second, but there is no change in the solution. To determine whether enough time elapses in the numerical simulation for vortices to develop, it is instructive to examine the time scale for vortex formation in the region of the shear layer just downstream of the dump plane. First, consider a typical vortex having a 1.0 cm diameter in this initial part of the shear layer. In addition, assume an average velocity of 1500 cm/sec in the vicinity of this developing vortex.¹ The time scale for formation should be the circumference of the vortex divided by the surrounding fluid velocity which is approximately 0.002 seconds. Based on this rough calculation, there appears to be sufficient time in the numerical calculation for large-scale vortices to develop in the shear layer.

1. Examination of the printed output from the stable flame calculation shows that at a point approximately 4.0 cm downstream of the dump plane, the shear layer width is about 1.5 cm and the average velocity across the shear layer is about 1500 cm/sec.

To substantiate the accuracy of the flashback calculation described in this section, a run is made in which the convergence criteria on pressure and temperature are lowered a whole order of magnitude (1×10^{-4} to 1×10^{-5} and 1×10^{-3} to 1×10^{-4} , respectively). This change yields no variation in the solution over that appearing in Figure 9.

So, this begs the question of what is causing the flashback in the calculated result. Is it a consequence of the approximately 30% increase in the amplitude of the acoustic oscillations? It should be noted here that the computed flashback result of Figure 9 is achieved using a partial donor-cell differencing scheme. When the quasi-second order upwind (QSOU) differencing scheme is used, the combustor and pre-mixer pressure oscillations are completely damped out and no flashback occurs for values of Φ up to approximately 0.7, beyond which no calculation is performed. A second run is made using the QSOU differencing scheme with a pre-exponential factor of 8.6×10^{11} , consistent with the Westbrook and Dryer one-equation global reaction rate mechanism for propane oxidation. Then the equivalence ratio is raised at a rate of 0.1 per second up to approximately 0.70 and, once again, neither pressure oscillations nor flashback occur. So, it is clear that the calculated flashback result of Figure 9 does depend on the differencing scheme used. For this computation, the QSOU differencing scheme is clearly more diffusive even though it is formally more accurate than the partial donor-cell method [3]. An implicit and otherwise unsubstantiated conclusion can be made from this dependence on the differencing scheme: since flashback never occurs (up to $\Phi \cong 0.70$) when acoustic pressure oscillations are damped out and does occur when there is a small increase in the amplitude of the oscillations, then perhaps this slight intensification of the acoustic field is the driving mechanism for flashback in the computed solution.

Regardless of whether this conclusion is valid or not, there does not appear in the calculated result the large, coherent vortices and the flame flickering mode observed in experiment

prior to flashback. Consequently, the complete instability mechanism described in section 1.3 is not accurately modeled in this calculation. As is mentioned in the next section in conjunction with decreasing the inflow velocity, this deficiency may be due in part to the spatial resolution of the premixer boundary layer and/or the $k - \epsilon$ turbulence model.

5.2 Decreased Inflow Velocity

As outlined in section 4.3, a second part of this analysis is to linearly decrease the inflow velocity while holding the equivalence ratio fixed at 0.44. Two separate calculations are made; one using the partial donor-cell differencing scheme and the other using the QSOU differencing scheme. It is found that, as the inflow velocity decreases, the high temperature gradient 'cone' seen in Figure 7 shortens and the combustor pressure decreases linearly, but no flame flickering or flashback occur. In each calculation, the inflow velocity is decreased at a rate of 750 cm/sec² to 1050 cm/sec, which is approximately half the original inflow velocity of 2133 cm/sec. Figure 11 presents the final segment of the combustor pressure history for the calculation using partial donor-cell differencing. It shows that there is no increase in the amplitude of the acoustic oscillations over that appearing in the latter part of Figure 8. In addition, it is interesting to note that the oscillations have become more irregular, an effect most likely caused by the increased influence of the step on the propagation of the acoustic waves.

Experimentally, when the inflow velocity is varied over a broad range, many turbulent shear layer instability frequencies result. This increases the likelihood that a constructive phase relationship will arise between the acoustic field and the shear layer instabilities as described in steps (1)-(3) of the instability mechanism in section 1.3. In an attempt to calculate a coupling between acoustic and shear layer oscillations, an additional computation is performed in which the inflow velocity is linearly increased from the stable flame result of Figure 7. Once again, two separate runs are made, one using partial donor

cell differencing and the other using QSOU differencing. In each calculation, the inflow velocity is increased at a constant rate of 1500 cm/sec^2 to a maximum of 4300 cm/sec , which is approximately twice the original inflow velocity of 2133 cm/sec . It is found that the high temperature gradient 'cone' elongates, as expected, and the combustor pressure increases linearly, but again no flame flickering or flashback occur.

Following are two possible explanations for the absence of combustion instabilities in the calculated result as the inflow velocity is varied. First, as is noted in step (2) of the instability mechanism in section 1.3, the velocity profile and flow structure of the premixer boundary layer affect the occurrence of combustion instabilities. The turbulent boundary layer in the premixer is thin and is therefore not spatially resolved by the boundary cells in the premixing region of the computational mesh. The law-of-the-wall boundary layer model describes the effects of turbulence on the wall shear stress and heat transfer coefficient but does not describe the turbulent boundary layer vortices themselves. The development and transport of these vortices may provide the seed for the development of coherent vortices in the shear layer downstream. To resolve turbulent boundary layer vortices, the mesh could be refined in the vicinity of all solid boundaries, but the expense of such a calculation would be extreme.

Before undertaking such an expensive calculation, a second possible explanation for the absence of vortices in the shear layer of the calculated result should be considered. The $k - \epsilon$ model has existed for some time [14] and it often does quite well to calculate a local value for the effective turbulent viscosity based on solutions to transport equations for turbulent kinetic energy and its dissipation rate. However, it has already been shown that the effects of numerical diffusion can play an important role in the occurrence of flashback, which indicates that this is a diffusion-sensitive phenomenon. The magnitude of turbulent diffusion may play a similarly important role in permitting/suppressing development of coherent vortices from shear layer instability. Development of a new turbulence model or

even refinement of the $k-\epsilon$ model parameters are beyond the scope of this work. Turbulence modeling is a difficult field and, despite the efforts of some of the best applied mathematicians, gains are made only very slowly.

CHAPTER 6

CONCLUSIONS AND RECOMMENDATIONS

6.1 Conclusions

A computed flashback sequence is achieved using the KIVA-II code by linearly increasing the equivalence ratio from the stable flame calculation of Figure 7. It is observed that the following two synergistic features that are identified experimentally by Proctor and T'ien and others do not appear in the calculated result:

- (1) the conception and growth of coherent vortices in the turbulent shear layer,
and;
- (2) high amplitude combustor pressure oscillations coincident with flame
flickering prior to flashback.

The absence of these features elicit the conclusion that the computational model does not accurately reproduce the experimental instability mechanism described in section 1.3. It is noted that the near-wall grid resolution and/or the $k-\epsilon$ turbulence model may be inadequate to simulate step (2) of this mechanism. This would then prevent the coupling of acoustic and shear layer frequencies as required for the conception of coherent vortices and, in turn, high amplitude combustor pressure oscillations. Also noted is the disparity in the time elapsed between the Proctor and T'ien experiment and the numerical calculation as the equivalence ratio is raised from 0.44 to the flashback limit. The question is raised as to whether vortices can form during the much shorter elapsed time of the numerical simulation. It is shown by means of a rough calculation of the time scale of vortex formation in the shear layer just downstream of the dump plane that sufficient time exists for the development of coherent vortices.

As mentioned in Chapter 5, the computed flashback result does depend on the finite differencing scheme used. The QSOU differencing scheme is more diffusive in this

calculation since it damps out the acoustic oscillations that occur when the partial donor-cell method is employed. That flashback occurs only when the acoustic oscillations are present leads to the conclusion that the intensification of the acoustic field resulting from the linear increase of the equivalence ratio may be the driving mechanism for the calculated flashback.

The inlet velocity is linearly decreased from the stable flame calculation of Figure 7 using both partial donor-cell and QSOU differencing, but neither an increase in the amplitude of the acoustic pressure oscillations nor flashback occur. In an attempt to induce coupling between the acoustic and shear layer oscillations as described in steps (1)-(3) of the instability mechanism in section 1.3, the inflow velocity is also increased over a broad range but no excitations are calculated. These results are attributed to the coarse spatial resolution of the premixer boundary layer and to uncertainty in the ability of the $k-\epsilon$ model to adequately simulate the small-scale turbulence in this boundary layer. As suggested previously, these features of the numerical model may preclude the development of turbulent shear layer instability waves which, in turn, would prevent the coupling of acoustic and shear layer oscillations necessary to form coherent vortices.

6.2 Recommendations for Further Analysis

Exit Aperture and the Acoustic Field

As noted in section 3.1, the exit aperture dimensions in the computational mesh are chosen so that the exit/combustion chamber cross-sectional area ratio correlates with the experiment. This properly models the incompressible flow resistance, but what of the acoustic field in the entire dump combustor?

The standing wave patterns comprising an acoustic field develop from the interference of longitudinally traveling waves that are reflected at each end of the dump combustor. The

nature of the reflections depends on the open-to-closed area ratios of the inlet and exit. As an illustration, consider a dump combustor in which the inlet geometry is held fixed while the exit dimensions are varied. When the end of the combustion chamber is completely closed (exhausting at another location), the fluid elements adjacent to the end wall are stationary (no slip at the wall), giving rise to an acoustic node. Conversely, the establishment of a completely open boundary at the end of the combustor would allow for nearly unrestricted movement of the fluid elements along the exit plane and an approximate antinode would occur. (A descriptive analogue is to consider the difference in the wave patterns for two longitudinally vibrating beams, one with both ends fixed and the other having one end free). Between these two extremes of fully closed to fully open are infinitely many exit geometries, each associated with a unique acoustic field. Therefore, the frequency of the standing wave fundamental and harmonic modes are a function not only of the length of the dump combustor, but also the inlet and exit dimensions.

In this analysis, the inlet geometry is easily specified since the experimental premixer is purely two-dimensional. Conversely, the geometry of the two-inch hole exhausting the experimental combustion chamber is three-dimensional and therefore more difficult to model acoustically. An even greater task, if at all possible in a two-dimensional analysis, is to select an exit geometry that simultaneously elicits the correct flow resistance and acoustic response. A compromise is made in this analysis by ensuring proper flow resistance while risking inaccuracy in modeling the acoustic response of the exit. Since the acoustic field is an important mechanism in the occurrence of flashback, this compromise may cause the computational model to depart significantly from the experiment. Consequently, if the Proctor and T'ien experiment is to be used as a basis for further numerical analysis, it is recommended that a three-dimensional model be developed. A simpler tactic would be to choose an experiment that uses an apparatus which has two-dimensional features throughout such as that in reference [12] (Karagozian, personal

correspondence). Perhaps then the CPU time and data storage that would have otherwise been consumed by computing in a three-dimensional volume could be utilized to refine the mesh in the boundary layer regions.

Symmetry Plane and the Acoustic Field

With the symmetry plane in the computational mesh, accurate simulation of transverse acoustic wave propagation and reflection is not possible in the numerical model. These acoustic waves are most likely present in the Proctor and T'ien experiment and may excite high frequency 'screech' modes of combustion instability. However, it is the lower frequency modes of instability induced by longitudinal acoustic wave propagation that have been the focus of recent experimental investigations [9,11,12,18-20] and which are described in the combustion instability mechanism in section 1.3. This being so, it is deemed worthwhile to continue to utilize a symmetry plane in further analysis. (Note: The asymmetries observed in Figure 5a are most likely a manifestation of asymmetric features of the Proctor and T'ien experimental rig such as the location of pressure transducers and stream thermocouples.)

Streaklines vs. Streamlines

Streamlines (loci of constant velocity gradient) are used to examine features of the velocity field, particularly the turbulent shear layer. In the review of this thesis, it was noted that the streamline plots may not reveal the large-scale coherent vortices associated with the combustion instability modes observed in experiment. Though not presented, velocity vector field plots are consistently used as an analytical tool to substantiate the streamline plots. In further analysis, however, it may be worthwhile to use plots of marker particle paths, or streaklines, since they may be more revealing than streamlines, particularly with regard to shear layer vortices.

Chemical Kinetics - One vs. Multi-Equation Model

The one-equation global reaction rate mechanism for propane oxidation developed by Westbrook and Dryer [15] appears to work well in this numerical analysis. A more rigorous test of this mechanism would be to see how well it models combustion within developing coherent vortices in the turbulent shear layer as predicted in step (3) of the instability mechanism in section 1.3. Unfortunately, as described in the previous chapter, coherent vortices do not appear in the shear layer of the calculated result. To say that this is a manifestation of the approximate nature of the global reaction rate mechanism is probably an overstatement. In fact, as suggested in the previous section, the disparity between the features of the calculated flashback sequence and those of the instability mechanism in section 1.3 is most likely due to the inability of the computational model to adequately simulate the first three steps in the mechanism that describe the coupling of acoustic and turbulent shear layer frequencies. This phenomenon is, of course, convective in nature and therefore not solely dependent on the reaction rate. However, since the reaction rate mechanism controls the rate of heat release from the oxidation of the fuel and this, in turn, governs the flame shape and structure, it may be worthwhile upon further analysis to incorporate a more elaborate reaction rate mechanism. The analyst will need to decide how much accuracy is gained for the added computing time required by a multi-equation reaction rate mechanism.

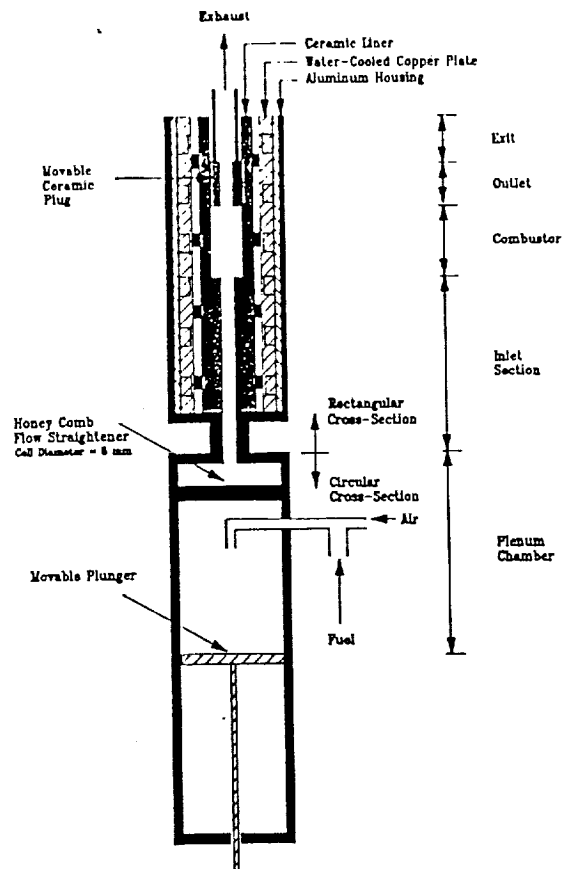


Figure 1a: Experimental Dump Combustor after Logan, et.al. [12]

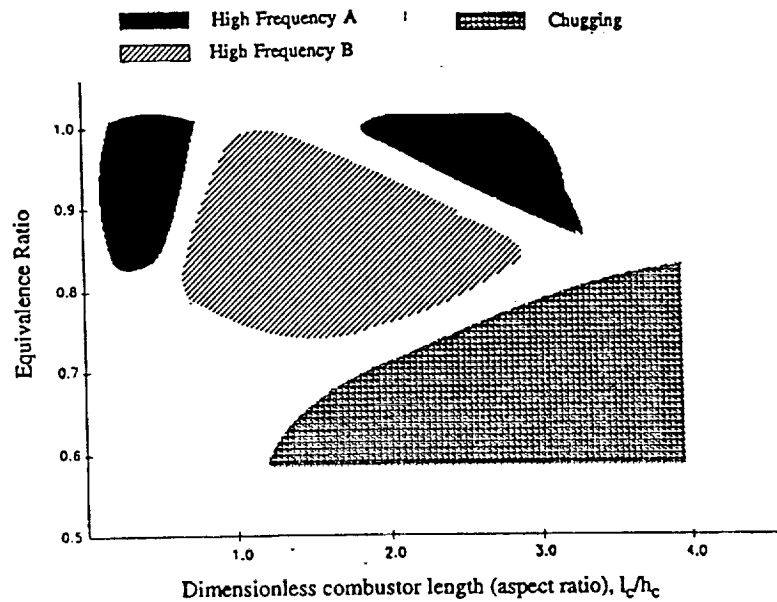


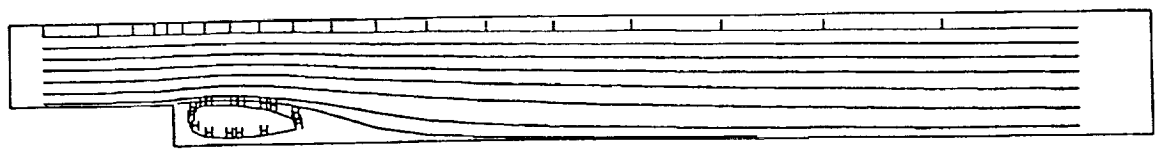
Figure 1b: Map of Combustor Modes after Logan, et. al. [12]

Figure 2a: KIVA-II - Turbulent Flow over a Step

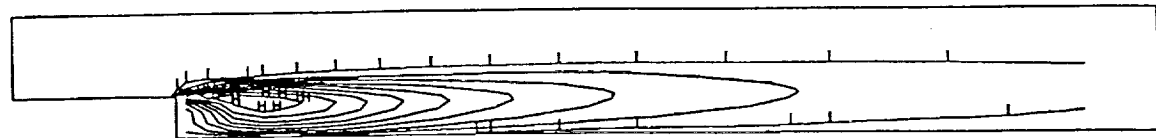


computational mesh

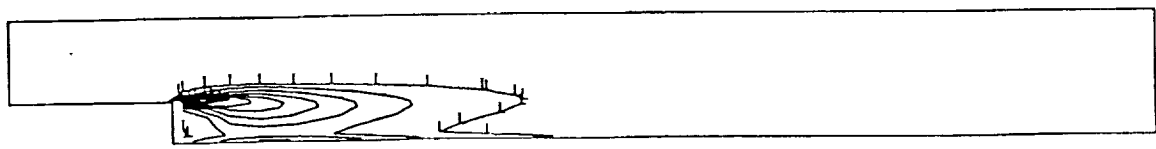
L - low contour line
H - high contour line



ncyc=15000 time=0.3160 streamlines min=0.176 max=13.425

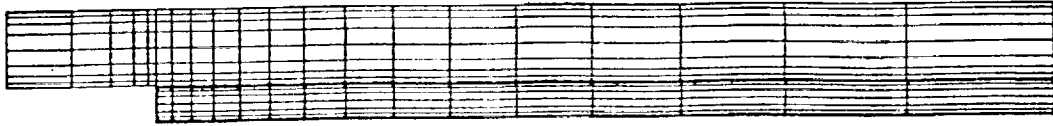


ncyc=15000 time=0.3160 turbulent kinetic energy min=78413.187 max=10956888.000

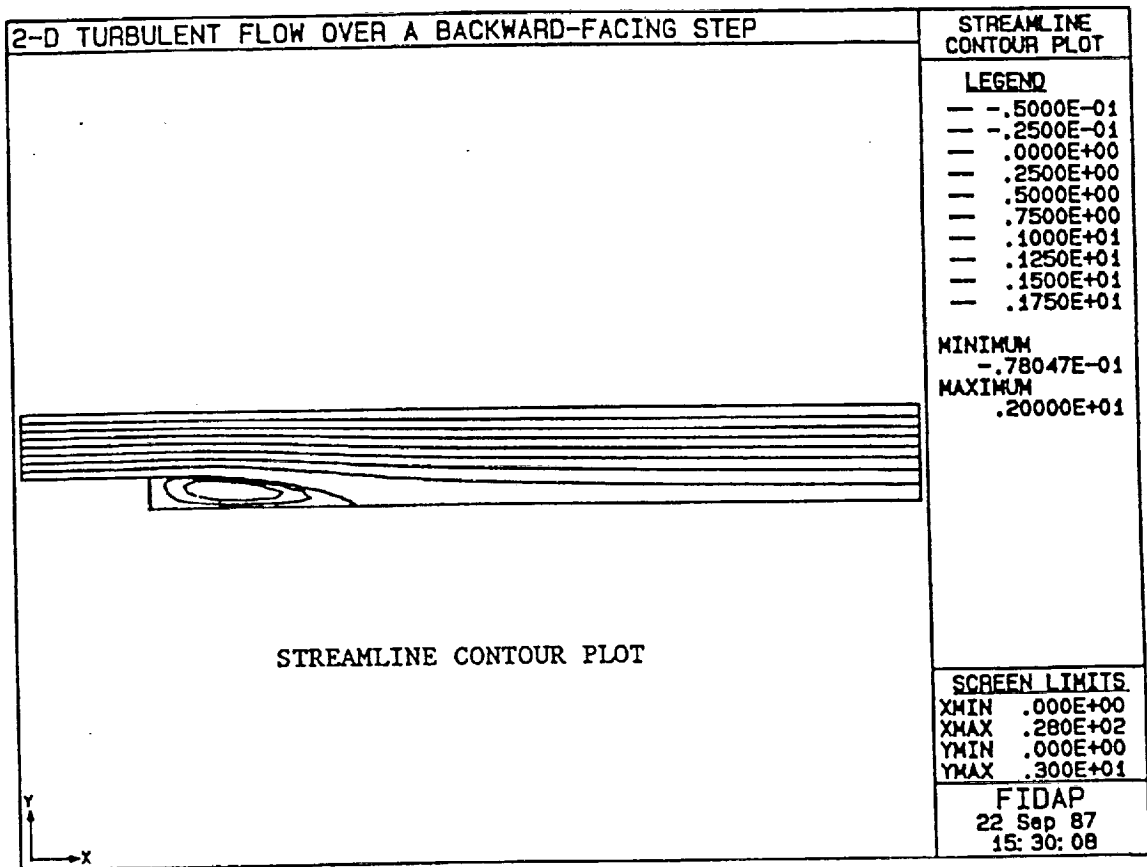


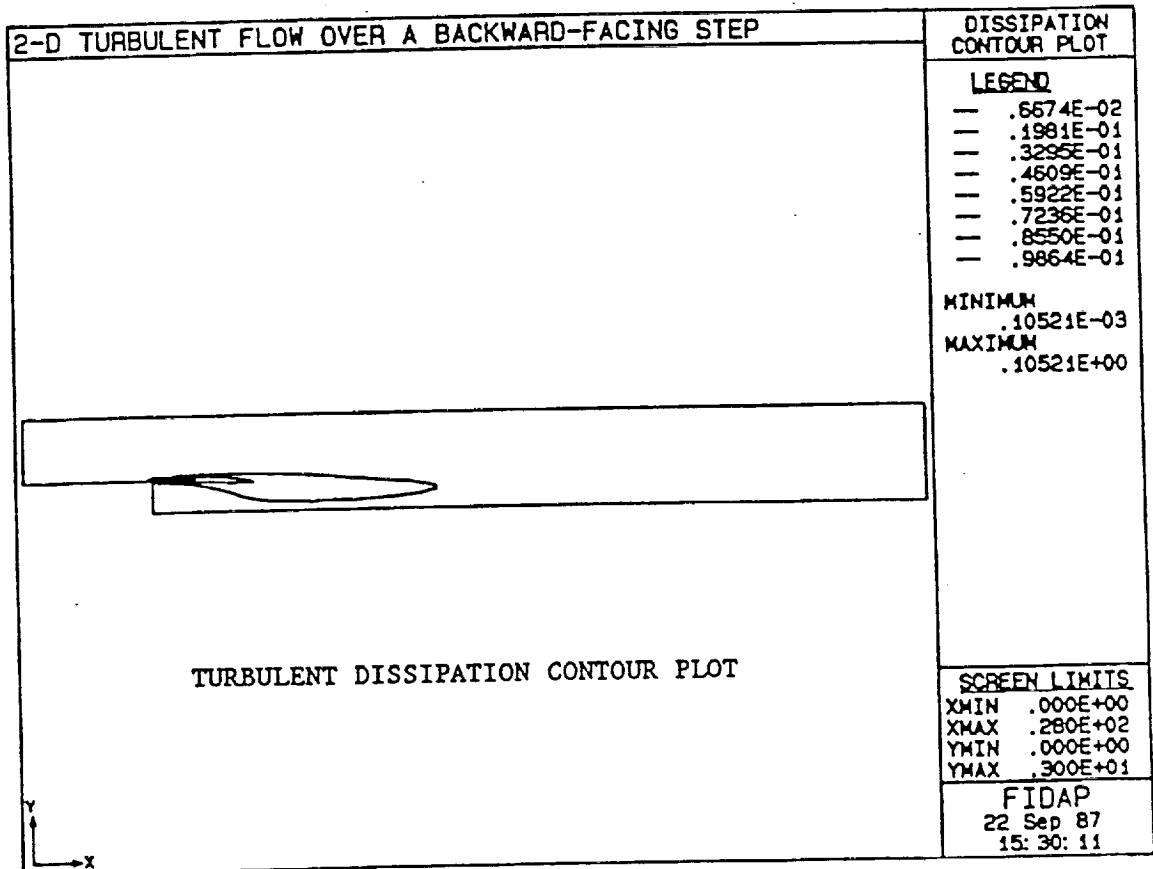
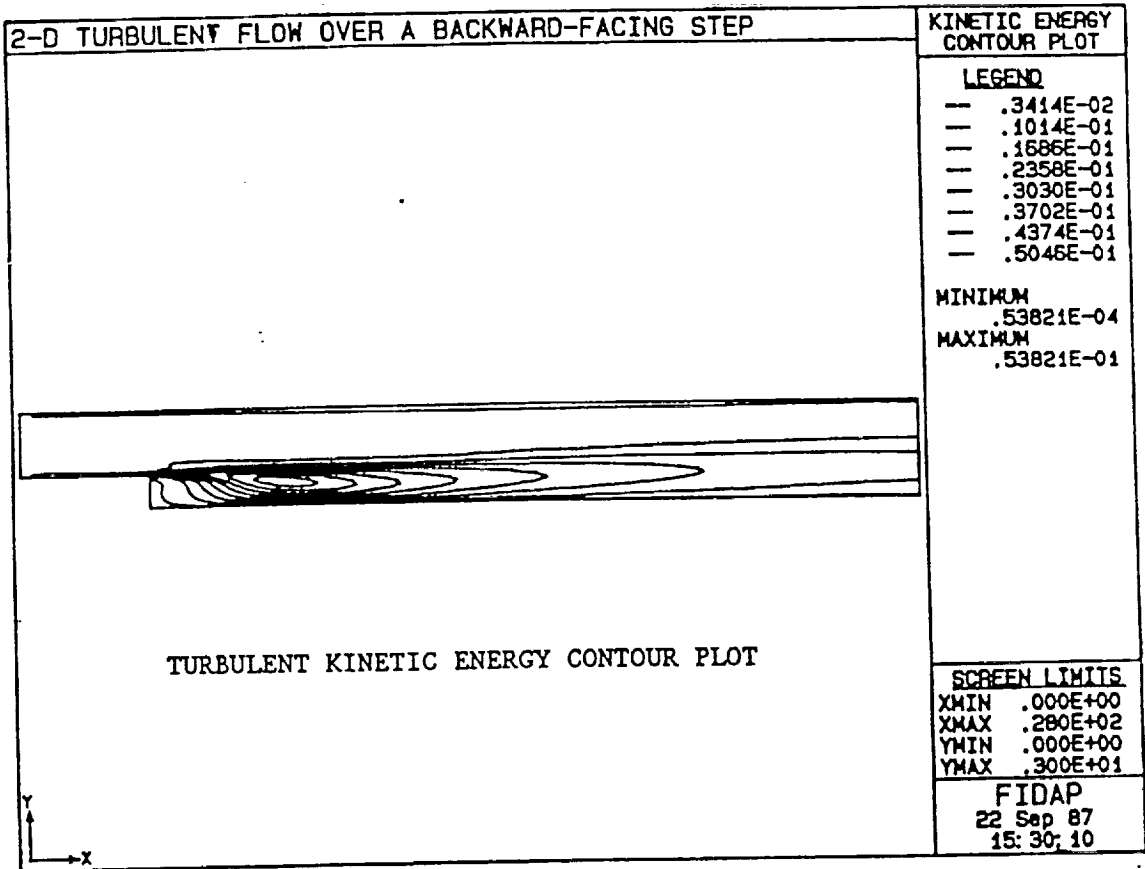
ncyc=15000 time=0.3160 t.k.e. dissipation rate min=31764096.0 max=64761268224.0

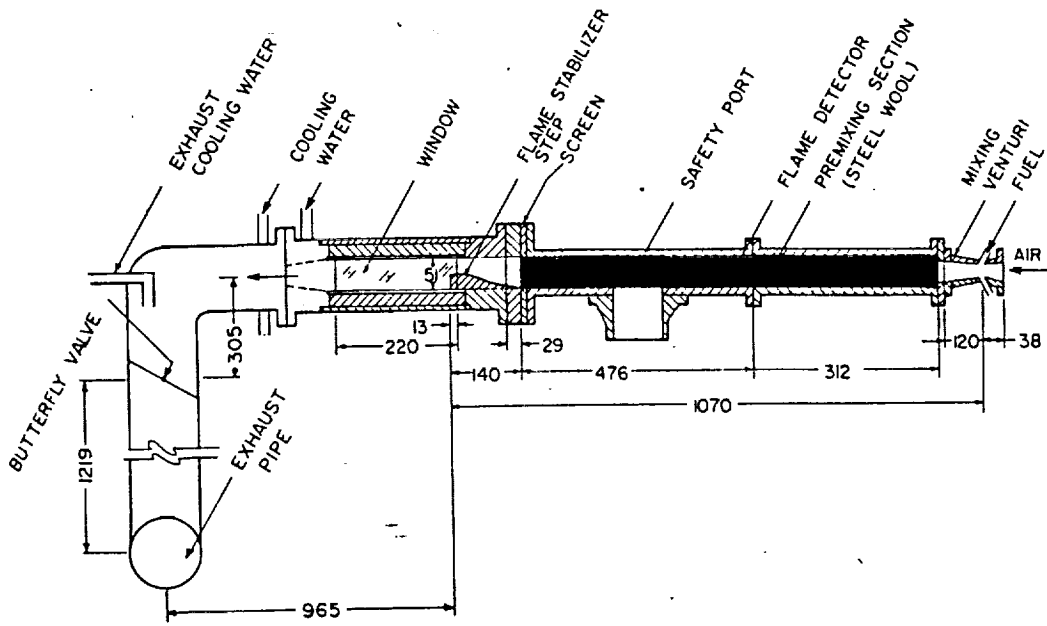
Figure 2b: FIDAP - Turbulent Flow Over a Step



GENERATED MESH







(5 ms between frames)

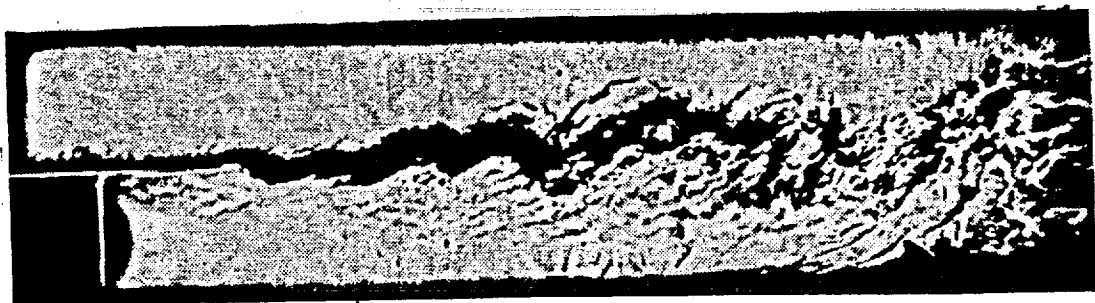
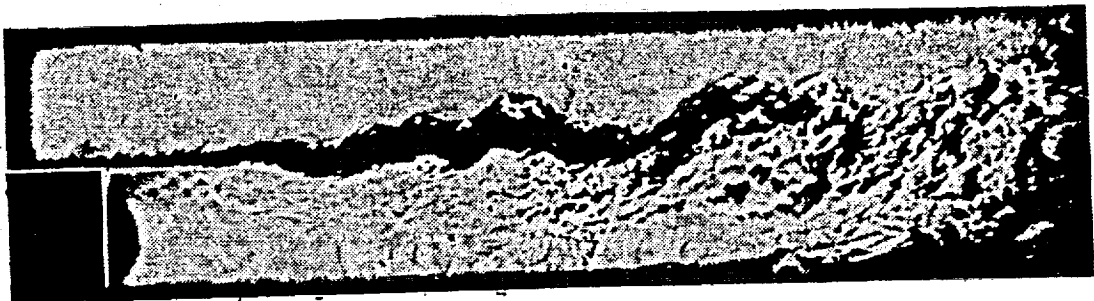
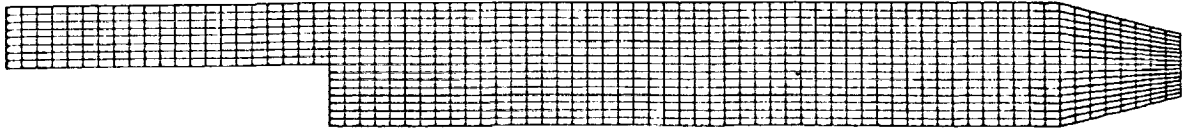
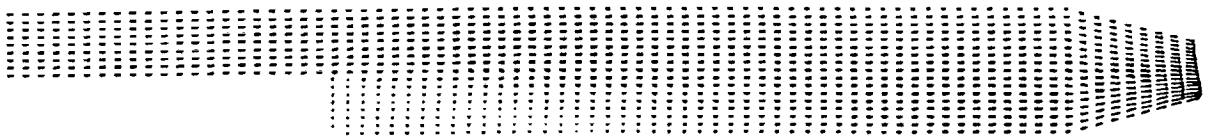


Figure 3a: Cinematographic Schlieren Record of Stable Combustion at $\Phi = 0.57$, after Keller, et.al.



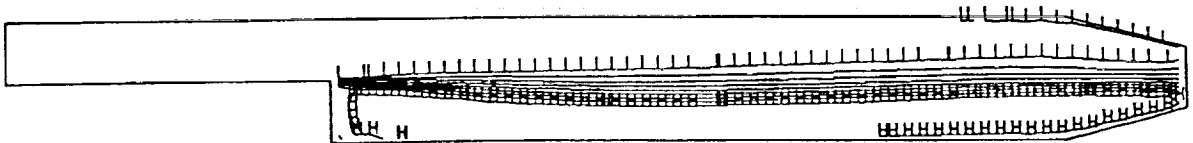
computational mesh



ncyc=3249 time=0.8524 sec velocity field velmax=4093 cm/sec

L - low contour line

H - high contour line



ncyc=3249 time=0.8524 sec temperature min=297.987 max=1628.848

Figure 3b: KIVA-II Numerical Model of Stable Flame in Fig. 3a

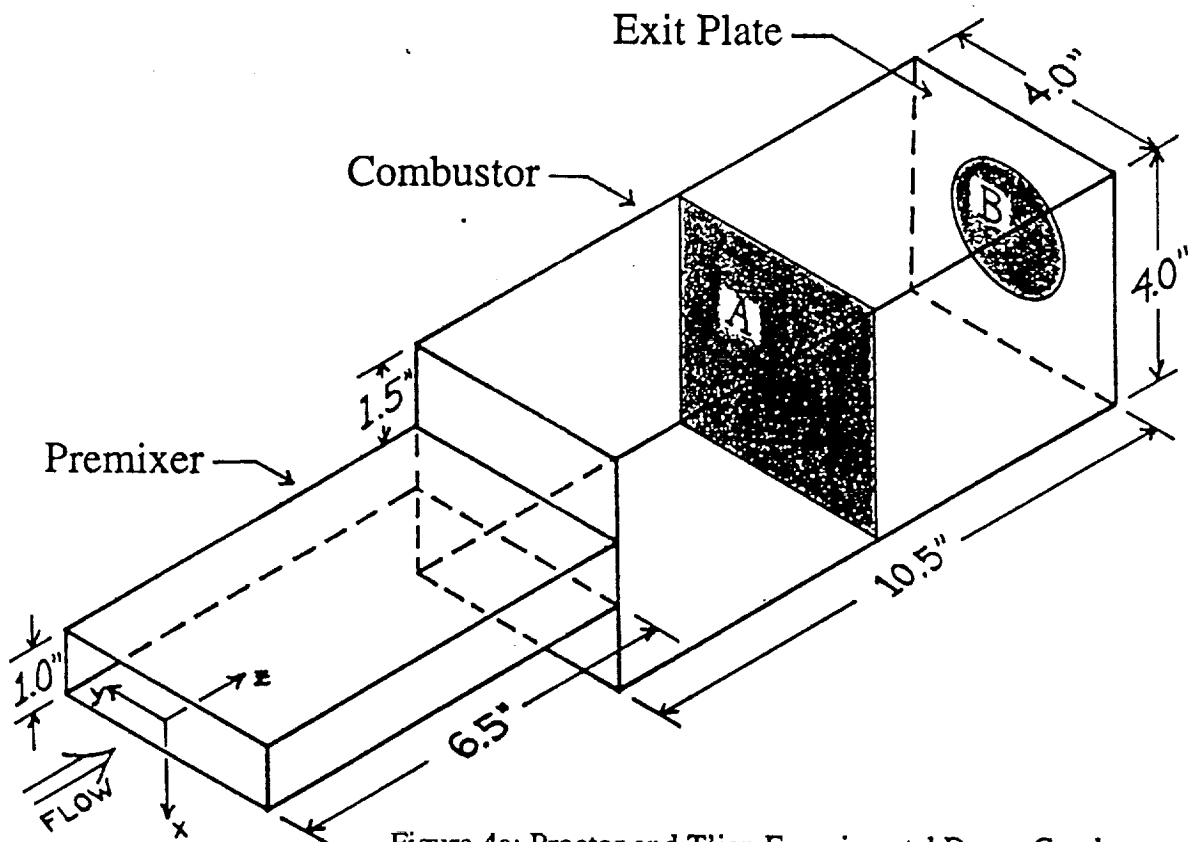


Figure 4a: Proctor and T'ien Experimental Dump Combustor

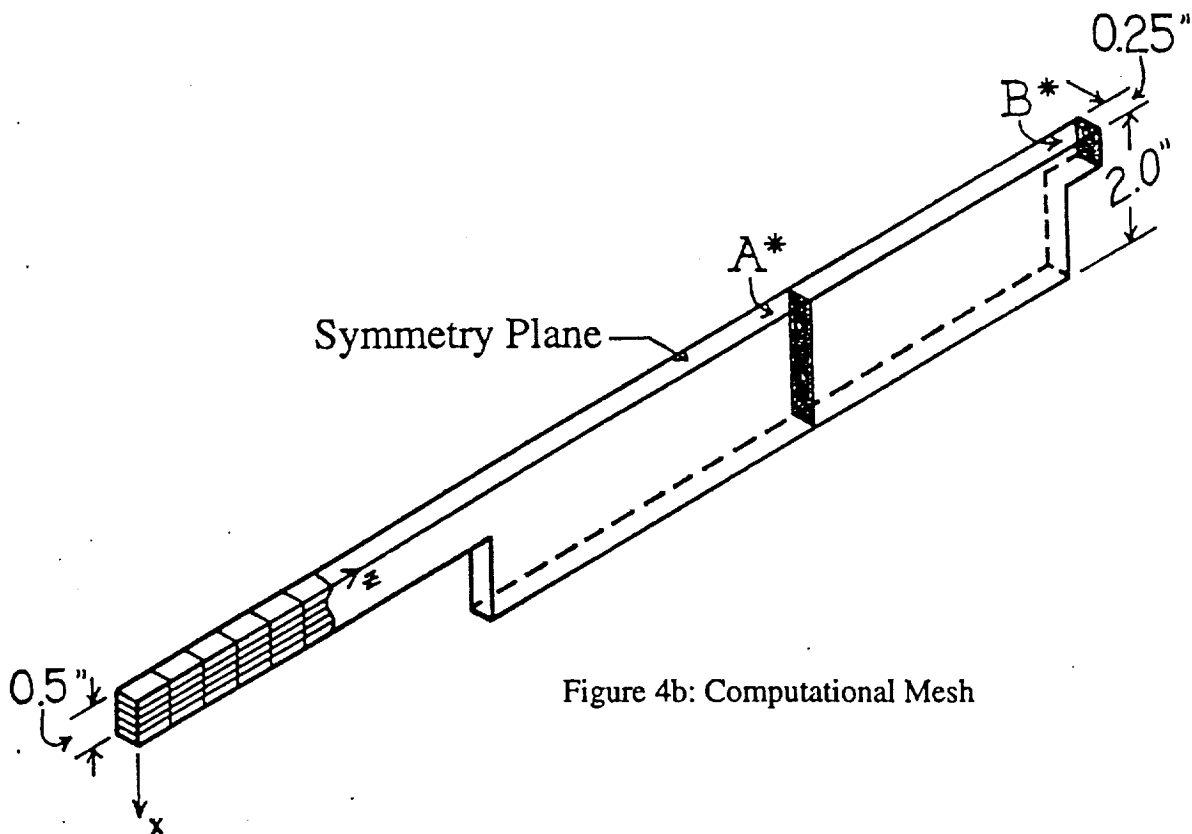
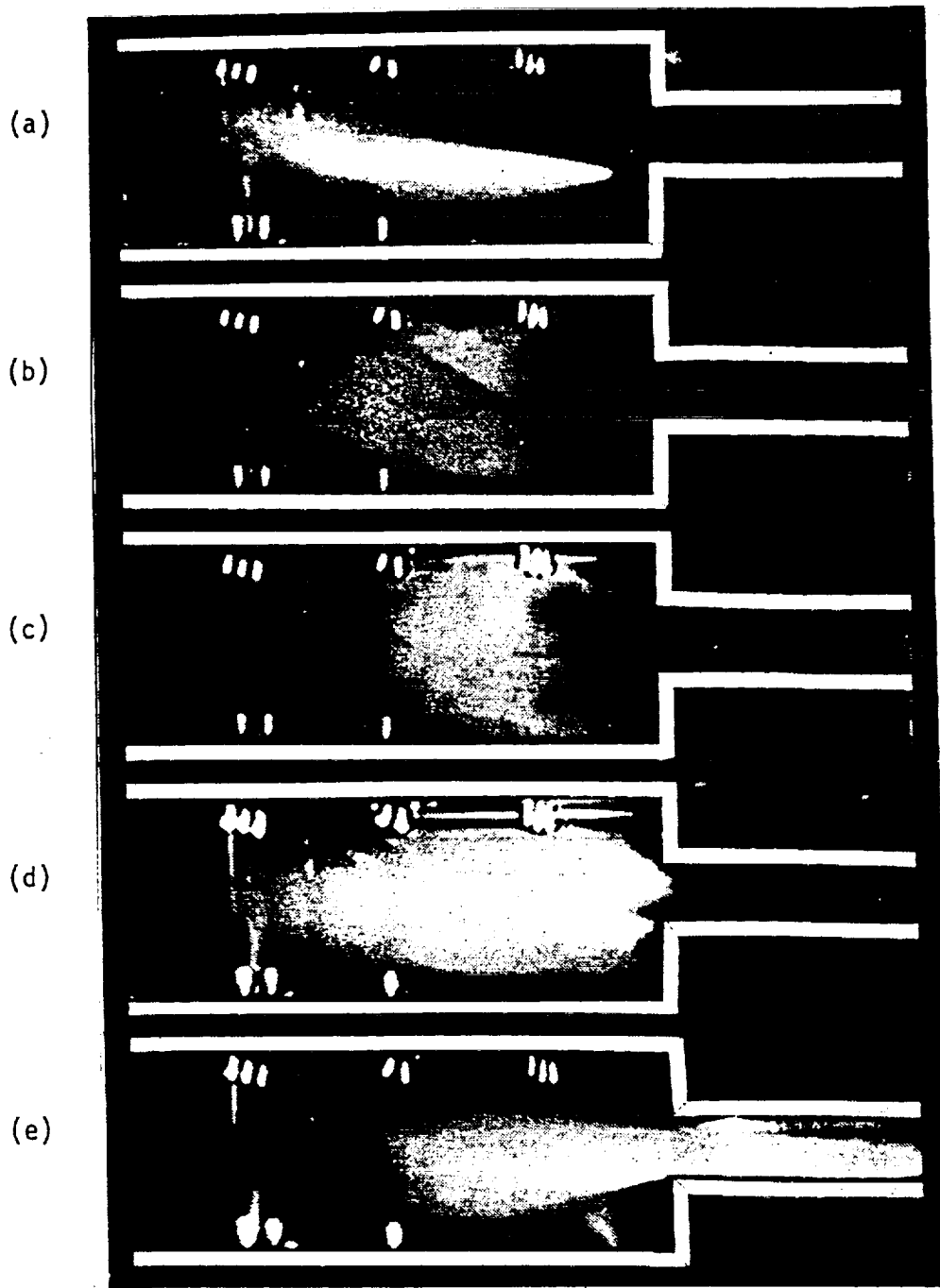


Figure 4b: Computational Mesh

Figure 5a: Proctor and T'ien Experimental Flashback Sequence



Different stages of burning. (a) and (b), lean flames, equivalence ratio, 0.41; (c) recirculation zones formed behind step, equivalence ratio, 0.44; (d) flame began flickering, equivalence ratio, 0.56; (e) maintained flashback, equivalence ratio, 0.60. Inlet air temperature, 850K; premixer wall temperature, 750K; average premixer velocity, 70 ft/s; fuel injector 8 in. upstream of step.

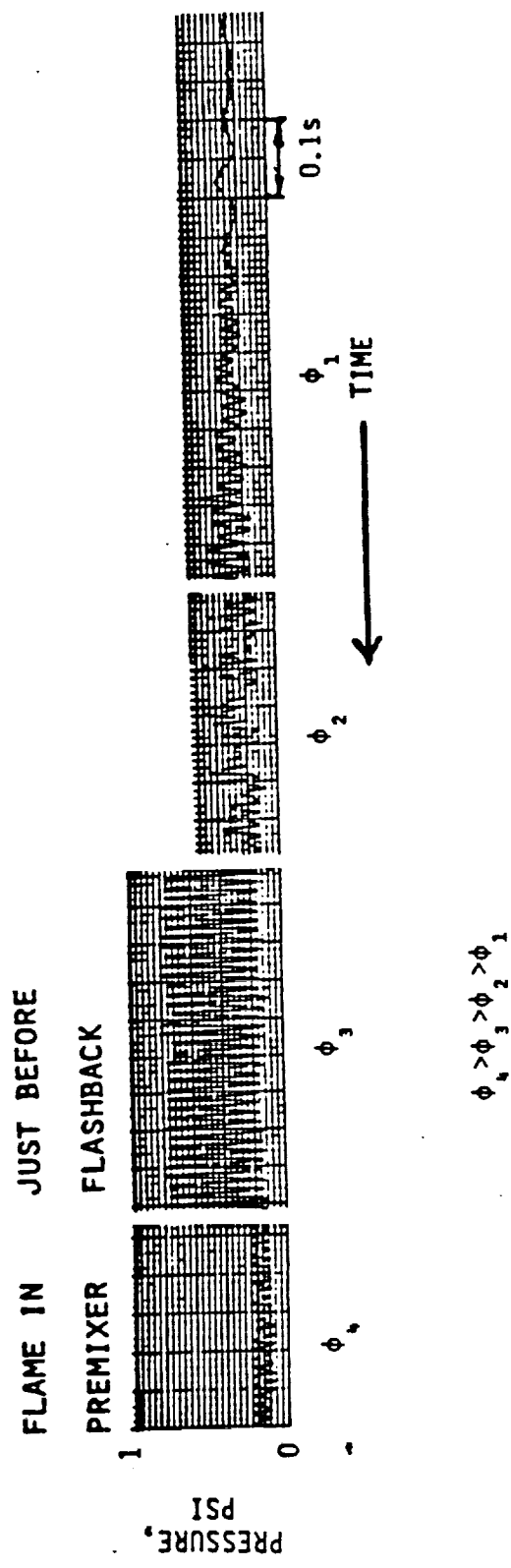
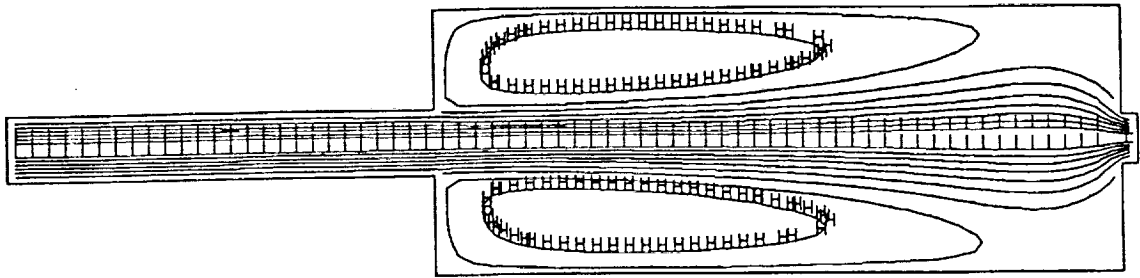


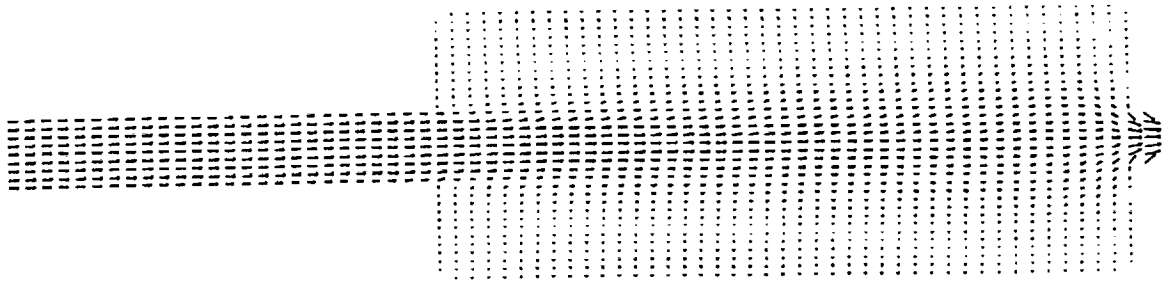
Figure 5b: Typical Combustor Pressure History as Equivalence Ratio is Increased, after Proctor and T'ien

L - low contour line

H - high contour line

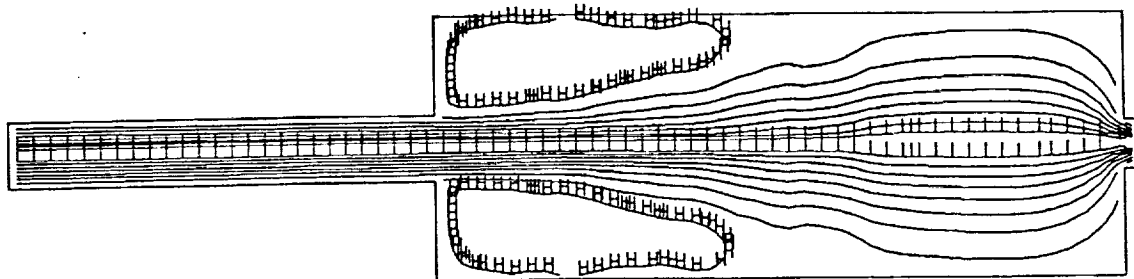


ncyc=1221 time=0.2159 sec streamlines min=0.044 max=0.745



ncyc=1221 time=0.2159 sec velocity field velmax=3982 cm/sec

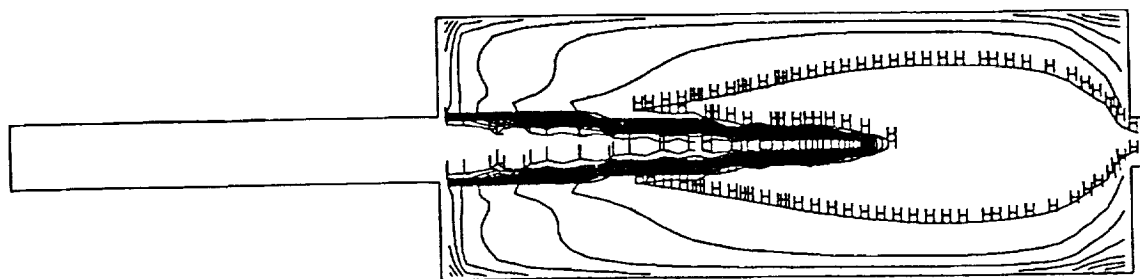
Figure 6: Cold Flow Steady State Calculation



ncyc=9816 time=0.8564 sec streamlines min=0.030 max=0.666

L - low contour line

H - high contour line



ncyc=9816 time=0.8564 sec temperature min=766.385 max=1798.5

Figure 7: Stable Flame Calculation at $\Phi = 0.44$

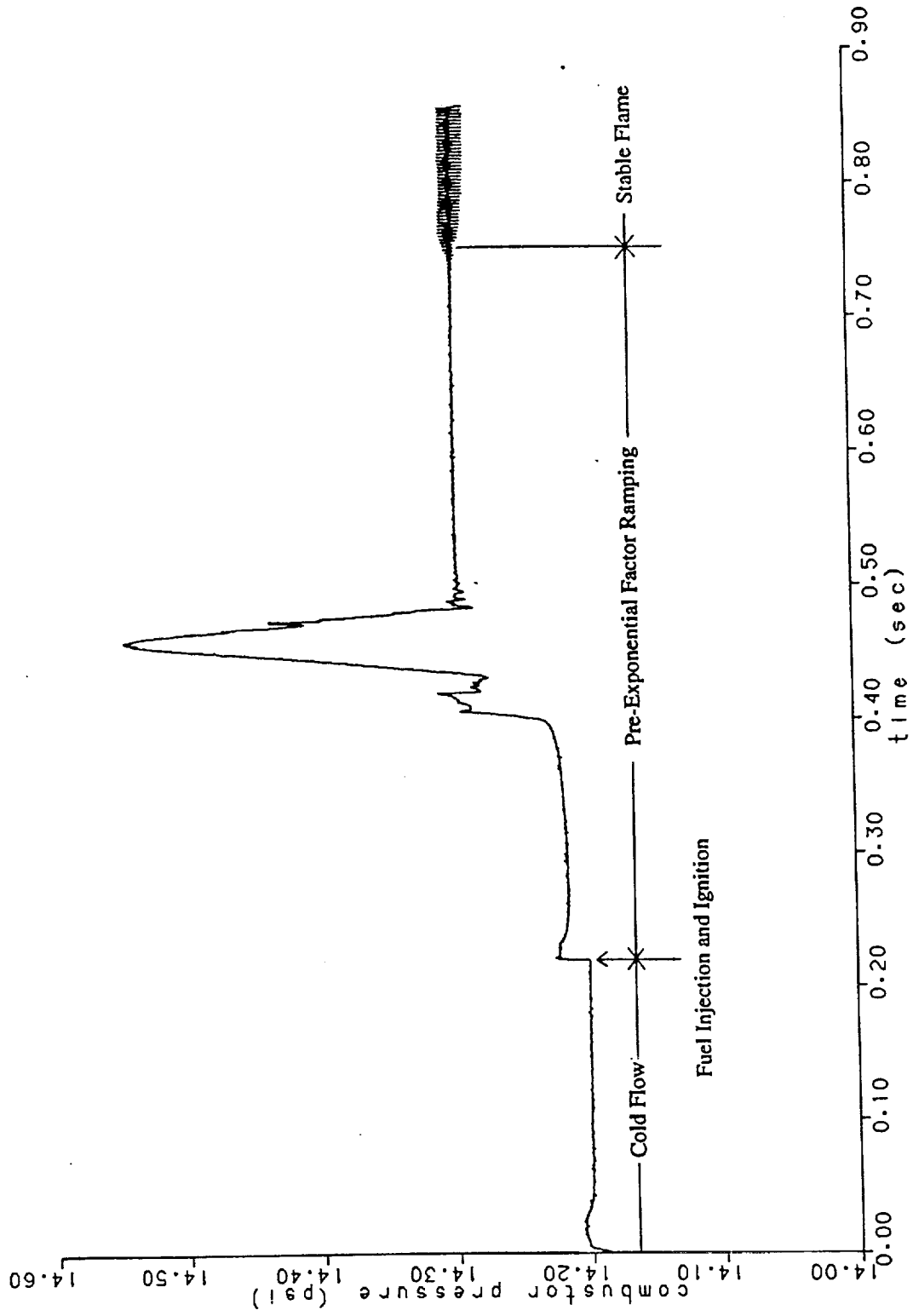
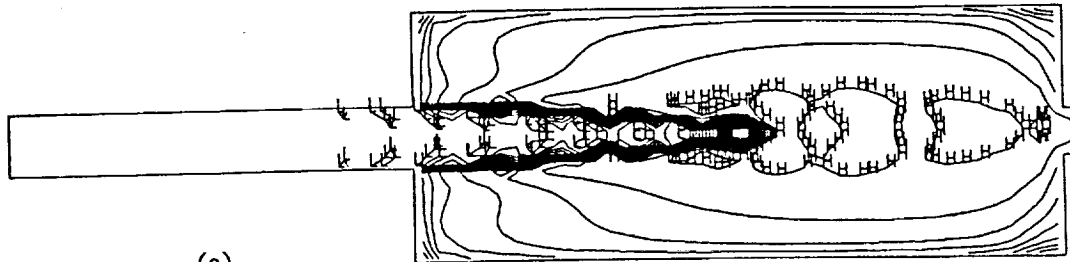


Figure 8: Combustor Pressure History of Reactive Flow Start-Up

Figure 9: Calculated Flashback Sequence

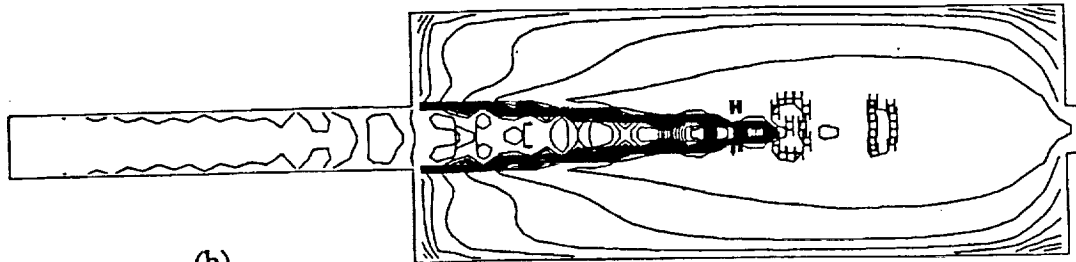
L - low contour line

H - high contour line



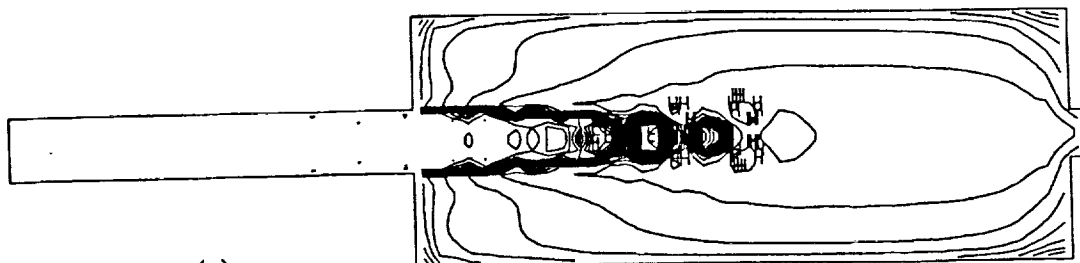
(a)

ncyc=29550 time=2.0009 sec temperature min=714.757 max=2063.4



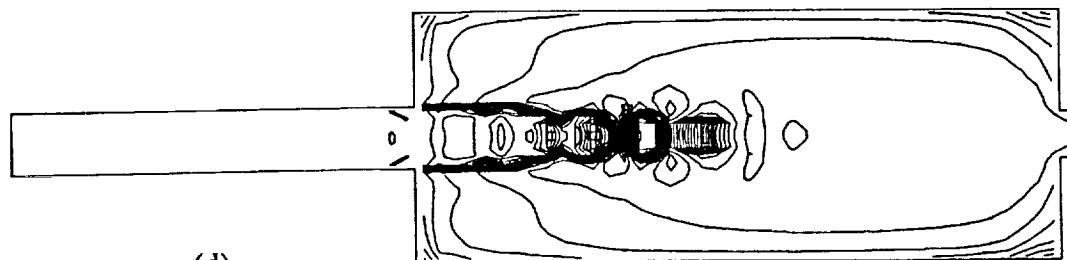
(b)

ncyc=29715 time=2.0099 sec temperature min=655.817 max=2099.6



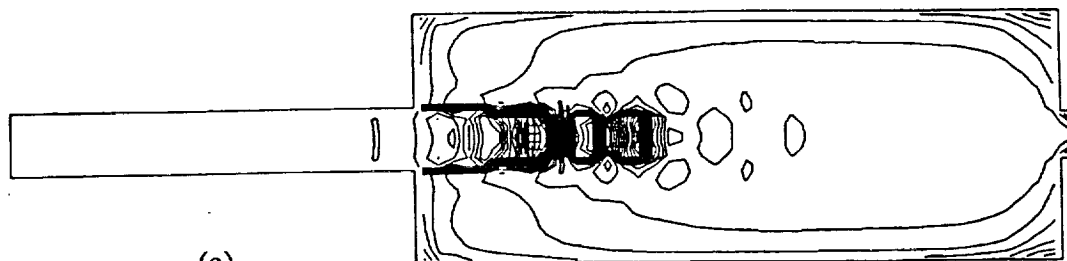
(c)

ncyc=29873 time=2.0184 sec temperature min=631.585 max=2109.0



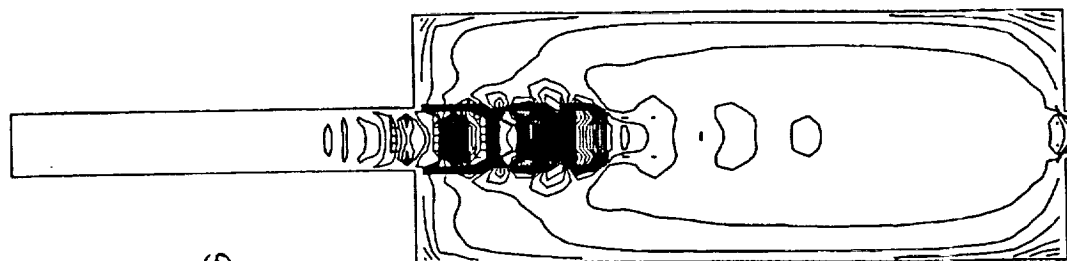
(d)

ncyc=29946 time=2.0224 sec temperature min=566.424 max=2251.3



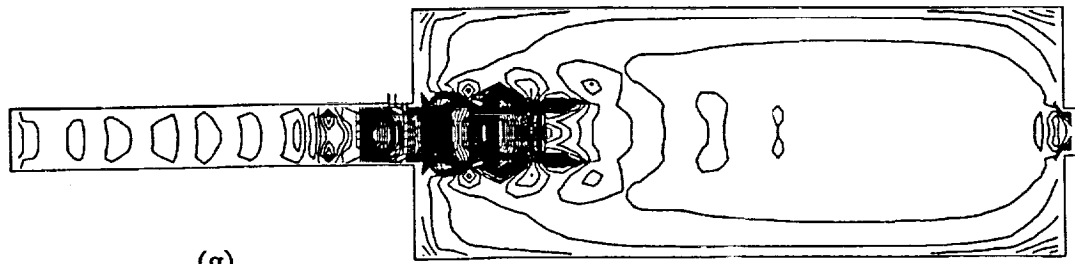
(e)

ncyc=29952 time=2.0262 sec temperature min=572.366 max=2251.8



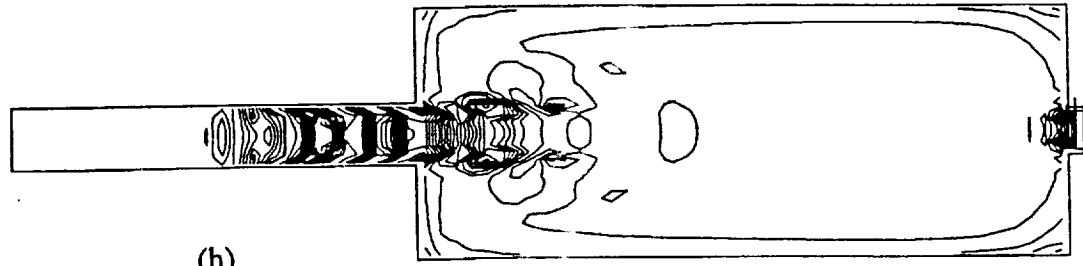
(f)

ncyc=30091 time=2.0302 sec temperature min=593.175 max=2251.0



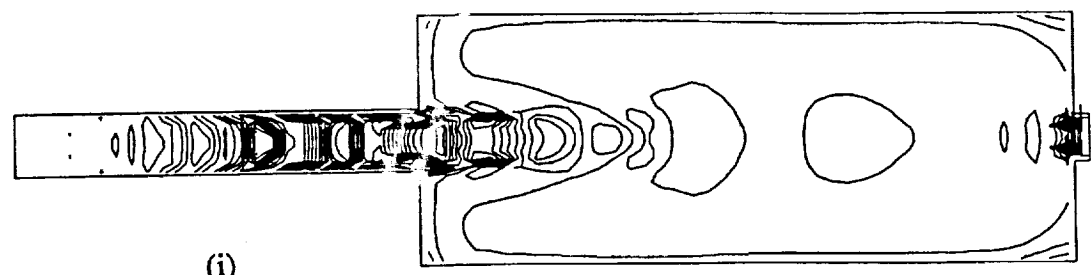
(g)

ncyc=30149 time=2.0331 sec temperature min=548.053 max=2254.7



(h)

ncyc=30211 time=2.0362 sec temperature min=345.690 max=2856.5

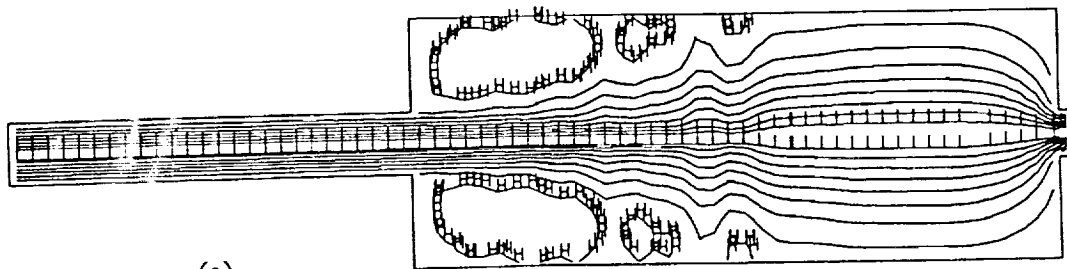


(i)

ncyc=30264 time=2.0366 sec temperature min=331.536 max=2981.9

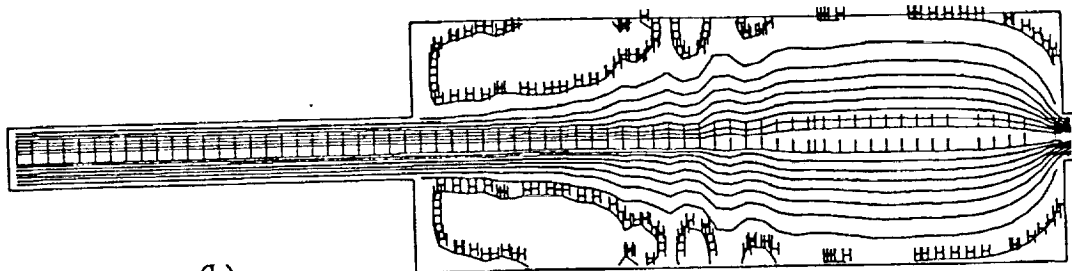
L - low contour line

H - high contour line



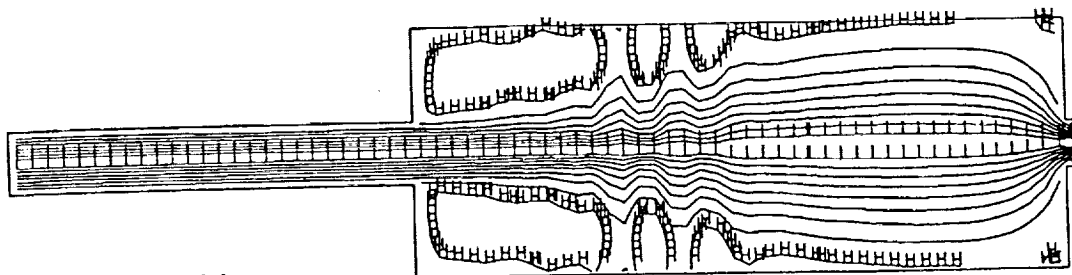
(a)

ncyc=24550 time=2.0009 sec streamlines min=0.028 max=0.678



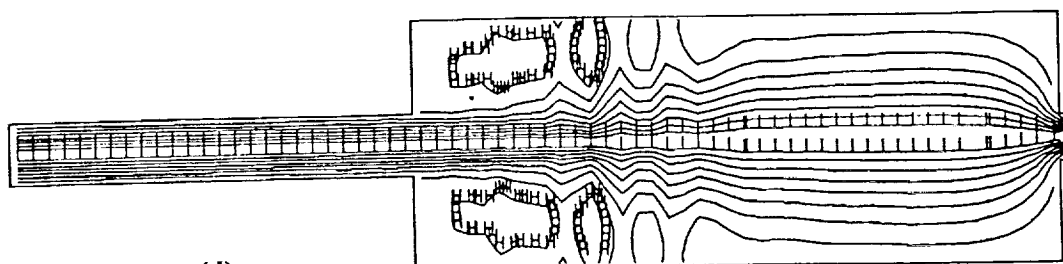
(b)

ncyc=29715 time=2.0099 sec streamlines min=0.028 max=0.674



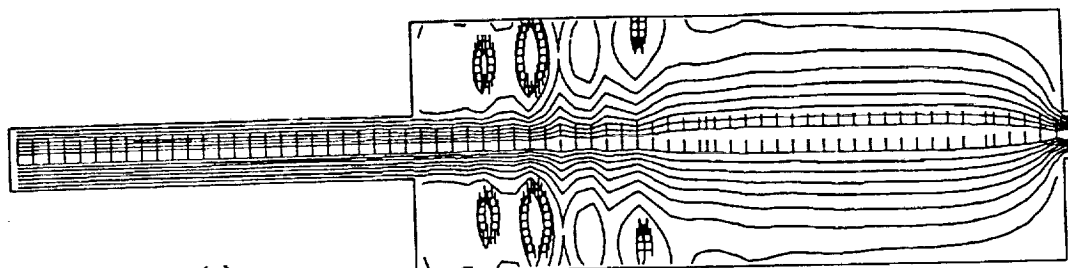
(c)

ncyc=29873 time=2.0184 sec streamlines min=0.029 max=0.673



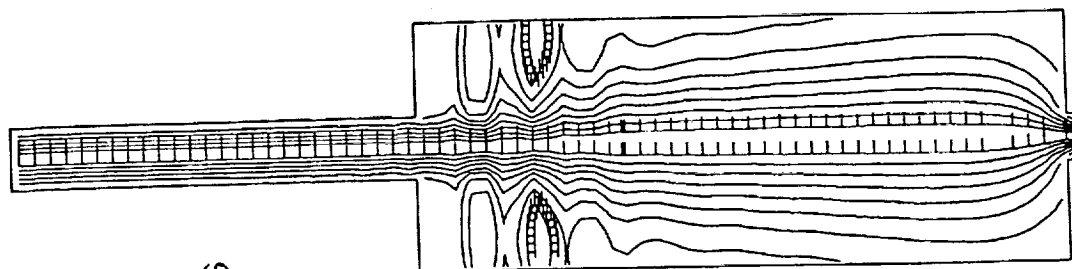
(d)

ncyc=29946 time=2.0224 sec streamlines min=0.028 max=0.687



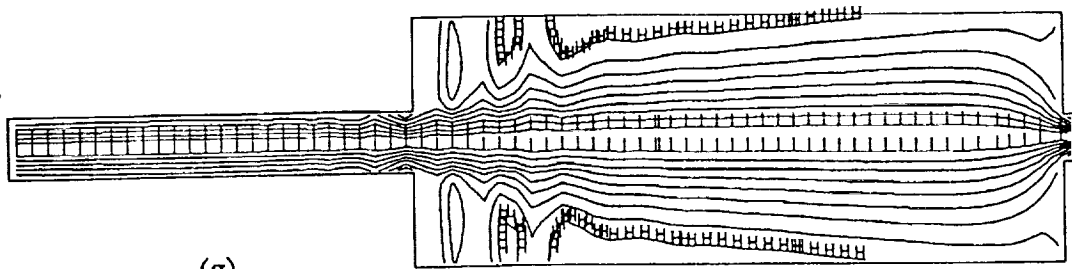
(e)

ncyc=29952 time=2.0262 sec streamlines min=0.028 max=0.710



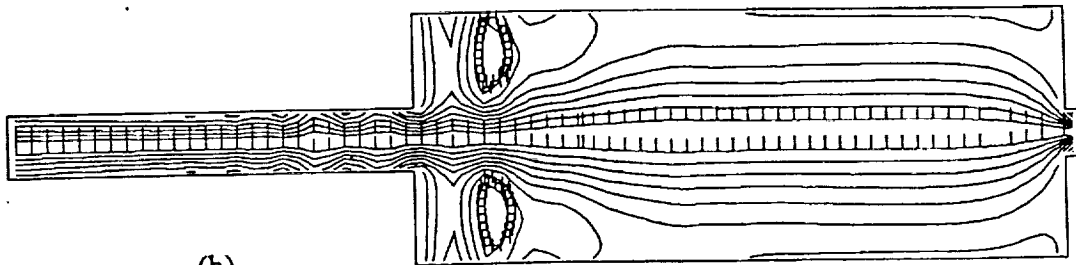
(f)

ncyc=30091 time=2.0302 sec streamlines min=0.038 max=1.050



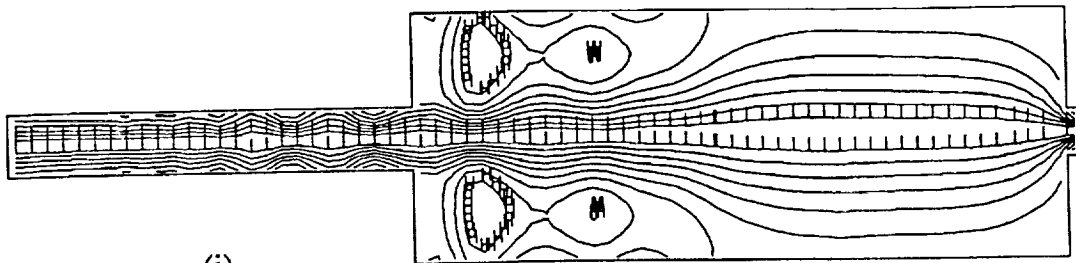
(g)

ncyc=30149 time=2.0331 sec streamlines min=0.036 max=0.905



(h)

ncyc=30211 time=2.0362 sec streamlines min=0.031 max=0.991



(i)

ncyc=30264 time=2.0396 sec streamlines min=0.027 max=0.921

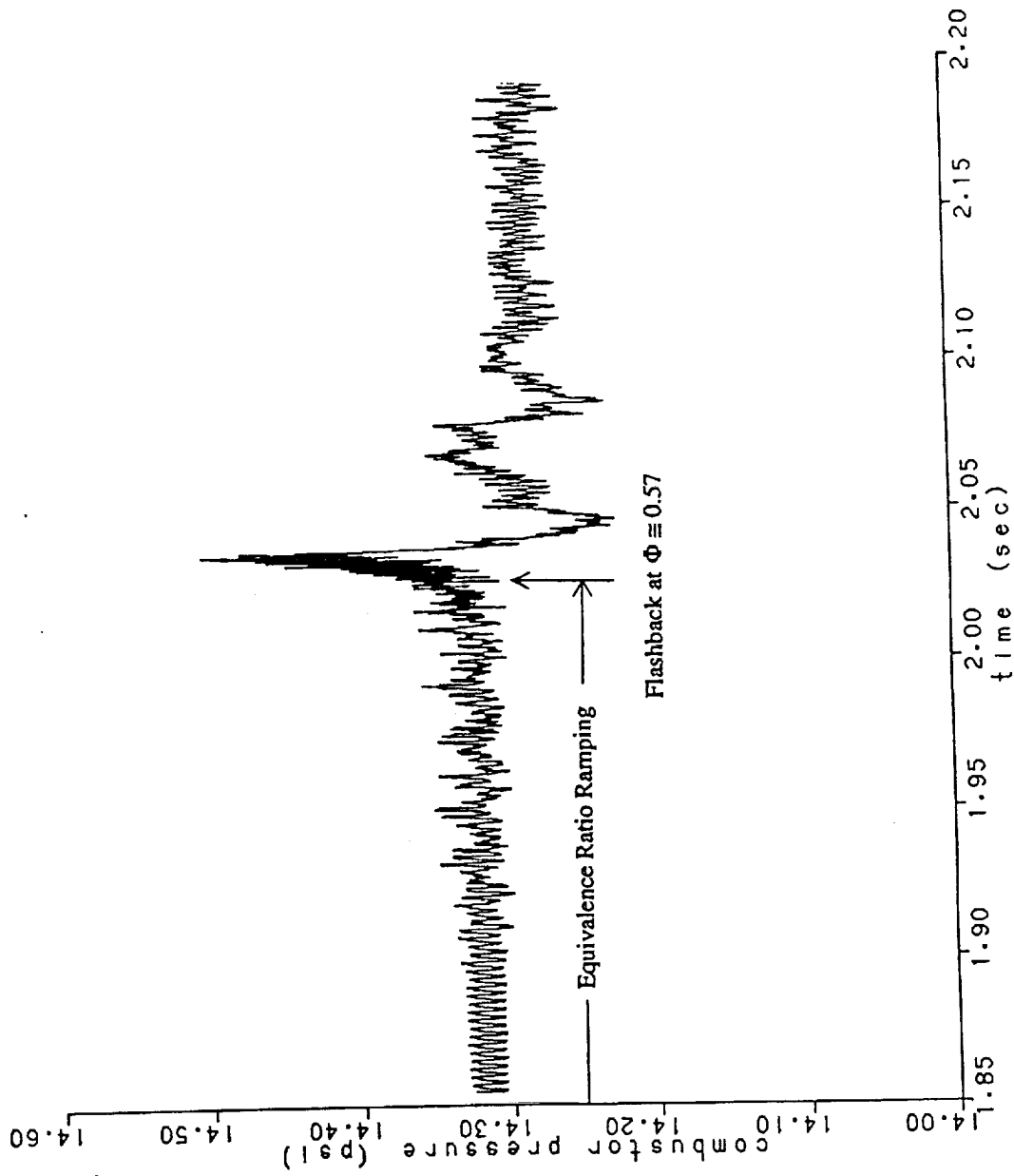


Figure 10: Combustor Pressure History of Flashback Sequence

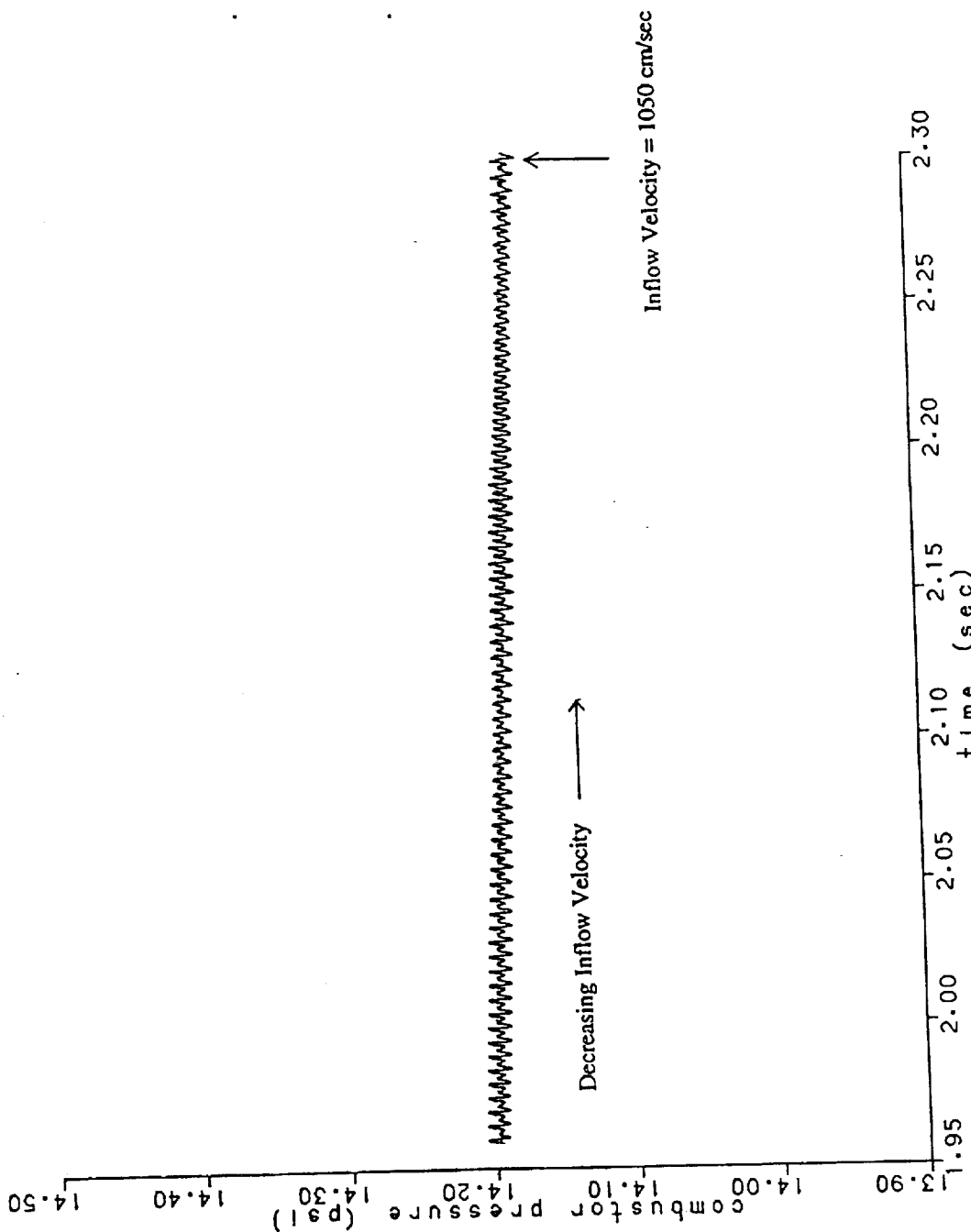
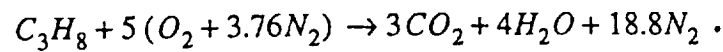


Figure 11: Combustor Pressure History as Inflow Velocity is Decreased

Appendix A

Appendix A shows the procedure used to compute inlet stagnation species densities of the reactant mixture. Inlet stagnation pressure and temperature remain constant in this study so the only variable in the following procedure is equivalence ratio. Note that superscript o identifies stagnation properties.

A stoichiometric reaction is first determined using a simple atomic balance:



The equivalence ratio Φ is defined on a mass basis as:

$$\Phi = \frac{\left(\frac{m_{fuel}}{m_{oxidant}} \right)_{actual}}{\left(\frac{m_{fuel}}{m_{oxidant}} \right)_{stoich}} .$$

Note that the oxidant is taken to be dry air ($O_2 + 3.76N_2$). Using the stoichiometric reaction above and the molecular weights of C_3H_8 , O_2 , and N_2 :

$$\left(\frac{m_{fuel}}{m_{oxidant}} \right)_{stoich} = 0.0641025 .$$

The following expression is derived for the stagnation species density of O_2 after defining a volume of mixture, V_{mix} , at the inlet and applying the equation of state there:

$$\rho_{O_2}^o = \frac{P_{mix}^o}{R_u T_{mix}^o} \left[\left(1 + 3.76 \frac{W_{N_2}}{W_{O_2}} \right) \frac{\Phi (0.0641025)}{W_{C_3H_8}} + \frac{4.76}{W_{O_2}} \right]^{-1} .$$

The species densities of C_3H_8 and N_2 are then determined using the following relations:

$$\rho_{C_3H_8}^o = (\rho_{O_2}^o + \rho_{N_2}^o) \Phi (0.0641025)$$


```
it=int(0.01*tin0)
elo=0.0
ehi=0.0
roin0=0.0
do 5270 isp=1,nsp
elo=elo+spdin0(isp)*ek(it+1,isp)
ehi=ehi+spdin0(isp)*ek(it+2,isp)
roin0=roin0+spdin0(isp)
5270 continue
csubv=0.01*(ehi-elo)/roin0
rgamin=1.0/(1.0+pin0/(roin0*csubv*tin0))
dprefin=botin*0.5*roin0*win**2
c
return
end
```

Appendix B

Appendix B shows segments of four subroutines in KIVA-II that required modification so that a symmetry plane could be used in the computational model. A simple change in the logical argument of each 'if' statement below treats the symmetry plane as if it were a symmetry axis in polar coordinates: adiabatic and impervious to mass, momentum, and turbulent kinetic energy transport. Note that the symmetry plane is located along the first radial plane ($i=1$).

Subroutine BCEPS:

```
c =20 if((i.eq.1.and.cyl.eq.0.) .or. (i.gt.1.and.f(i4-1).eq.0.)) then
      20 if((i.eq.1.and.cyl.eq.1.) .or. (i.gt.1.and.f(i4-1).eq.0.)) then
          if4=i4
          go to 30
      elseif((i.eq.nx .and. rtout.eq.0.) .or. (i.lt.nx .and. f(i1).eq.0.))
```

Subroutine BCRESE:

```
c === efacik=cvmgt(0.0,efacik,i.eq.1 .and. cyl.eq.0.0)
      efacik=cvmgt(0.0,efacik,i.eq.1 .and. cyl.eq.1.0)
      efacik=cvmgt(0.0,efacik,i.gt.1 .and. f(i4-1).eq.0.0)
      efacik=cvmgt(0.0,efacik,i.eq.nx .and. rtout .eq.0.0)
      efacik=cvmgt(0.0,efacik,i.lt.nx .and. f(i4+1).eq.0.0)
```

Subroutine LAWALL:

```
c =40 if((i.eq.1.and.cyl.eq.0.) .or. (i.gt.1.and.f(imjk).eq.0.)) goto 50
      40 if((i.eq.1.and.cyl.eq.1.) .or. (i.gt.1.and.f(imjk).eq.0.)) goto 50
          if((i.eq.nx .and. rtout.eq.0.0) .or.
             & (i.lt.nx .and. f(i1).eq.0.0)) go to 60
          go to 80
```

Subroutine SETUP:

```
c === if((i.eq.1 .and. cyl.eq.0.) .or.
          if((i.eq.1 .and. cyl.eq.1.) .or.
          & (i.gt.1 .and. f(i4-1).eq.0.)) go to 5110
          if(icart3.eq.0) go to 5140
          if(j.eq.1 .or. f(i4-nxp).eq.0.) go to 5120
          if(j.eq.ny .or. f(i4+nxp).eq.0.) go to 5130
```

Appendix C

The stable flame calculation of Figure 7 exhibits acoustic oscillations that are seen in the latter part of Figure 8. As noted in section 5.1, these oscillations increase in amplitude as the equivalence ratio is raised linearly in time. Figure 10 shows the acoustic disturbances as they become irregular prior to flashback. To show that these oscillations are acoustically driven, the following calculation is made:

Assume the fluid in the dump combustor is air at 1200K. The speed of sound c in the fluid is then:

$$c = \sqrt{\gamma RT} = \sqrt{(1.4) \left(\frac{8.3143 \times 10^7}{28.97} \right) (1200)} \cong 70,000 \text{ cm/sec}$$

where the value 28.97 is the molecular weight of air which is needed for proper unit cancellation.

Define T as the period of the regular, symmetric oscillations seen in Figures 7 and 10:

$$T = \frac{0.05 \text{ sec}}{19 \text{ cycles}} = 0.0026 \text{ sec} .$$

Note that an accurate reading of the number of cycles occurring in 0.05 seconds is obtained from pressure history plots representing the time interval between Figures 7 and 10. In the interest of brevity, these plots are not presented.

The overall length of the dump combustor is 43.18 cm. Define t^* as the time elapsed as a sound wave travels this distance:

$$t^* = \frac{43.18 \text{ cm}}{70,000 \text{ cm/sec}} .$$

The inlet in the computational model is velocity specified and can therefore be considered

an acoustic node. Conversely, the outlet, being pressure specified, is considered an approximate antinode. Consequently, a quarter wave exists in the computational mesh so that t^* must be multiplied by 4 to determine the period of acoustic oscillations, defined as τ below:

$$\tau = 4 \times t^* = 0.0025 \text{ sec .}$$

Finally, comparing T with τ , it can be seen that the oscillations are acoustic.

Appendix D

The input file used in the computations relating to the Proctor and T'ien experiment is listed below. There are a few variables that are added to the original KIVA-II input file for this analysis. Shown first is a description of these supplemental variables and then the input listing.

nctap9 cycle interval between writes to post-processing file tape9.
 nc1st beginning cycle for history plot arrays.
 fturb multiplicative factor used to determine the influence of effective turbulent
 viscosity on the reactive flow calculation. Appears only in subr. VISC:

$$\text{terme} = \text{fturb} * \text{cmu} * \text{tke}(\text{i4}) ** 2 * \text{ro}(\text{i4}) / \text{epsden}$$

 where terme is the effective turbulent viscosity term in the equation for
 $\text{amu}(\text{i4})$, the cell-specific bulk fluid viscosity.
 t1fuel time at which fuel is fluxed in with dry air at the inlet plane.
 winrate rate of linear increase in inflow velocity, win.
 eqrate rate of linear increase in inflow equivalence ratio, eqrin.
 pin0 stagnation pressure upstream of the inlet plane.
 spdin1-12 species stagnation densities upstream of the inlet plane.

Also, as noted in section 4.1, the pre-exponential factor $\text{cf}(1)$ for the fuel oxidation reaction is linearly increased in time during ignition. This is accomplished at the beginning of subroutine CHEM as follows:

```
if(t.gt.t1ign .and. cf(1).lt.1.9e+11)
&  cf(1)=(1.9e+11/0.60)*(t-t1ign)
```

Activation temperature $\text{ef}(1)$, temperature exponent $\text{zetaaf}(1)$, and species concentration exponents $\text{ae}(\text{isp},1)$ are obtained from reference [15].

maine k053190 16x1x69 2-d proctor, w/ pdc, chemeq 053190

irest	25
ipost	1
nx	16
ny	1
nz	69
lwall	1
nchop	0
lpr	1
jsectr	0
irez	0
ncfilm	99999
nctap8	99999
nctap9	99999
nclst	45317
nclast	99999
cafilm	9.99e+9
cafin	9.99e+9
cadump	9.99e+9
dcadmp	9.99e+9
angmom	0.0
cyl	0.0
dy	0.5
pgssw	0.0
sampl	0.0
dti	1.04167e-4
dtmxca	9.99e+9
dtmax	9.99e+9
tlimd	3600.0
twfilm	9.99e+9
twfin	9.99e+9
fchsp	0.25
stroke	9.55
squish	0.181934
rpm	0.0
atdc	0.0
conrod	16.269
offset	0.0
swirl	0.0
swipro	0.00
thsect	360.0
epsy	1.0e-3
epsv	1.0e-3
epsp	1.0e-4
epst	1.0e-3
epsk	1.0e-3
epse	1.0e-3
gx	0.0
gy	0.0
gz	0.0
tcylwl	750.0
thead	750.0
tpistn	750.0
tvalve	750.0

tempi	800.0
pardon	1.0
a0	0.0
b0	1.0
anc4	0.05
adia	0.0
anu0	0.0
fturb	1.0
visrat	-.66666667
tcut	900.0
tcute	1200.0
epschm	0.02
omgchm	1.0
tkei	4.55e+4
tkesw	1.0
sgsl	0.0
uniscal	0.0
airmu1	1.457e-5
airmu2	110.0
airla1	252.0
airla2	200.0
expdif	0.6
prl	0.74
rpr	1.11
rprq	1.0
rpre	0.769231
rsc	1.11
xignit	1.50e+3
tlfuel	2.20e-1
tlign	2.20e-1
tdign	0.20
calign	9.99e+9
cadign	9.99e+9
iignl1	1
iignr1	2
jignf1	1
jignd1	1
kignb1	32
kignt1	32
iignl2	0
iignr2	0
jignf2	0
jignd2	0
kignb2	0
kignt2	0
kwikeq	1
numnoz	1
numvel	1
injdist	1
kolide	0
tlinj	-1.0
tdinj	-1.0
calinj	9.99e+9
cadinj	9.99e+9

References

1. Smith, O.I., Marchant, R., Willis, J., Lee, L.M., and Karagozian, A.R., "Incineration of Surrogate Wastes in a Low-Speed Dump Combustor," *Combust. Sci. & Tech.*, Vol. 74, 1990, pp. 199-210.
2. Culick, F.E.C., "Combustion Instabilities in Propulsion Systems," *Combustion Instabilities Driven by Thermo-chemical Acoustic Sources*, presented at ASME Winter Meeting, San Francisco, 1989.
3. Amsden, A.A., Butler, T.D., and O'Rourke, P.J., "KIVA-II: A Computer Program For Transient Multidimensional Chemically Reactive Flows With Sprays," SAE Technical Paper No. 872072, Toronto, Ontario, 1987.
4. Roshko, A., "Structure of Turbulent Shear Flows: A New Look," *AIAA Journal*, Vol. 14, Oct. 1976, pp.1349-1357.
5. Davies, P.O.A.L, and Yule, A.J., "Coherent Structures in Turbulence," *J. Fluid Mech.*, Vol. 69, 1975, pp. 513-537.
6. Brown, G.L. and Roshko, A., "On Density Effects and Large Structures in Turbulent Mixing Layers," *J. Fluid Mech.*, Vol. 64, 1974, pp. 775-816.
7. Ganji, A.R. and Sawyer, R.F., "Experimental Study of the Flowfield of a Two-Dimensional Premixed Turbulent Flame," *AIAA Journal*, Vol. 18, July 1980, pp.817-824.
8. Keller, J.O., Vaneveld, L., Korschelt, D., Hubbard, G.L., Ghoniem, A.F., Daily, J.W., and Oppenheim, A.K., "Mechanism of Instabilities in Turbulent Combustion Leading to Flashback," *AIAA Journal*, Vol, 20, Feb., 1982, pp. 254-262.
9. Smith, D.A. and Zukoski, E.E., "Combustion Instability Sustained by Unsteady Vortex Combustion," AIAA Paper No. 85-1248, Monterey, Calif., July, 1985.
10. Lord Rayleigh, *The Theory of Sound*, Vol. II, MacMillen & Co., Ltd., 1896, pp. 226-227.

11. Schadow, K.C., Gutmark, E., Parr, T.P., Parr, D.M., Wilson, K.J., and Crump, J.E., "Large Coherent Structures as Drivers of Combustion Instability," *Combust. Sci. & Tech.*, Vol. 64, 1989, pp. 167-186.
12. Logan, P., Lee, J.W., Lee, L.M., and Karagozian, A.R., "Acoustics of a Low-Speed Dump Combustor," to appear in *Combust. & Flame*, 1991
13. Proctor, M.P. and T'ien, J.S., "Combustor Flame Flashback," NASA Report No. CR-174961, 1985.
14. Jones, W.P. and Launder, B.E., "The Prediction of Laminarization with a Two-Equation Model of Turbulence," *Int. Jour. of Heat and Mass Transfer*, Vol. 15, 1972, pp. 301-314.
15. Westbrook, C.K. and Dryer, F.L., "Chemical Kinetic Modeling of Hydrocarbon Combustion," *Prog. Energy Combust. Sci.*, Vol. 10, 1984, pp. 1-57.
16. Pitz, R.W. and Daily, J.W., "Combustion in a Turbulent Mixing Layer Formed at a Rearward-Facing Step," *AIAA Journal*, Vol. 21, Nov. 1983, pp. 1565-1570.
17. Lee, S.T. and T'ien, J.S., "A Numerical Analysis of Flame Flashback in a Premixed Laminar System," *Combust. & Flame*, Vol 48, 1989, pp. 273-285.
18. Poinset, T.J., Trouve, A.C., Veynante, D.P., Candel, S.M., and Esposito, E.J., "Vortex-driven Acoustically Coupled Combustion Instabilities," *J. Fluid Mech.*, Vol. 177, 1987, pp. 265-292.
19. Poinset, T.J. and Candel, S.M., "A Nonlinear Model for Ducted Flame Combustion Instabilities," *Combust. Sci. & Tech.*, Vol. 61, 1988, pp. 121-153.
20. Sterling, J.D. and Zukoski, E.E., "Longitudinal Mode Combustion Instabilities in a Dump Combustor," 25th AIAA Aerospace Sciences Mtg., AIAA Paper No. 87-0220.
21. Lewis, B. and von Elbe, G., *Combustion, Flames and Explosions of Gases*, 3rd Edition, Academic Press, Inc., 1987, pp. 233-236.
22. Glassman, I., *Combustion*, 2nd Edition, Academic Press, Inc., 1987.
23. Lefebvre, A., *Gas Turbine Combustion*, Hemisphere Publishing Corp, 1983.